

# Aligning Machine and Human Visual Representations across Abstraction Levels

Lukas Muttenthaler<sup>1,2,3,\*</sup>, Klaus Greff<sup>1</sup>, Frieda Born<sup>2,3,4</sup>, Bernhard Spitzer<sup>4</sup>, Simon Kornblith<sup>5</sup>, Michael C. Mozer<sup>1</sup>, Klaus-Robert Müller<sup>1,2,3,6,7,\*</sup>, Thomas Unterthiner<sup>1</sup> and Andrew K. Lampinen<sup>1,\*</sup>

<sup>1</sup>Google DeepMind, <sup>2</sup>Machine Learning Group, Technische Universität Berlin, <sup>3</sup>BIFOLD, Berlin Institute for the Foundations of Learning and Data, Berlin, Germany, <sup>4</sup>Max Planck Institute for Human Development, Berlin, <sup>5</sup>Anthropic, <sup>6</sup>Department of Artificial Intelligence, Korea University, Seoul, <sup>7</sup>Max Planck Institute for Informatics, Saarbrücken, Germany, \* corresponding authors

Deep neural networks have achieved success across a wide range of applications, including as models of human behavior in vision tasks. However, neural network training and human learning differ in fundamental ways, and neural networks often fail to generalize as robustly as humans do, raising questions regarding the similarity of their underlying representations. *What is missing for modern learning systems to exhibit more human-like behavior?* We highlight a key misalignment between vision models and humans: whereas human conceptual knowledge is hierarchically organized from fine- to coarse-scale distinctions, model representations do not accurately capture all these levels of abstraction. To address this misalignment, we first train a teacher model to imitate human judgments, then transfer human-like structure from its representations into pretrained state-of-the-art vision foundation models. These human-aligned models more accurately approximate human behavior and uncertainty across a wide range of similarity tasks, including a new dataset of human judgments spanning multiple levels of semantic abstractions. They also perform better on a diverse set of machine learning tasks, increasing generalization and out-of-distribution robustness. Thus, infusing neural networks with additional human knowledge yields a *best-of-both-worlds representation* that is both more consistent with human cognition and more practically useful, thus paving the way toward more robust, interpretable, and human-like artificial intelligence systems.

*Keywords:* AI alignment, human cognition, representation learning, computer vision

## 1. Introduction

While deep learning has recently driven rapid progress in areas of artificial intelligence such as natural language processing [LeCun et al., 2015; Brown et al., 2020] and computer vision [Radford et al., 2021; Dosovitskiy et al., 2020; Zhai et al., 2023; Kirillov et al., 2023], even the best of these systems often fail in ways that humans would not [Lapuschkin et al., 2016; Geirhos et al., 2018; Lapuschkin et al., 2019; Geirhos et al., 2020; Hermann et al., 2019; Thrush et al., 2022; Bowers et al., 2022; Muttenthaler et al., 2023b; Hermann et al., 2023]. These failures have led to renewals [Lake et al., 2017; Bowers et al., 2022] of older arguments that neural networks lack essential ingredients of human intelligence [Fodor and Pylyshyn, 1988; Marcus, 1998; McClelland et al., 2010; Holyoak and Hummel, 2014; Tenenbaum et al., 2011]. How can we build systems that have more human-like behavior?

Human perception is robust to changes in the environment and generalizes across different visual settings [Lake et al., 2015, 2017; Roads and Mozer, 2017; Geirhos et al., 2018; Lake and Baroni, 2023]. However, model performance declines—often drastically—if the data distribution between training and test sets is shifted [e.g., Sugiyama et al., 2007; Sugiyama and Kawanabe, 2012; Geirhos et al., 2020; Hendrycks et al., 2021a]. This lack of robustness in the representations of vision models poses a challenge for many downstream applications that require the ability to generalize [e.g., Lapuschkin et al., 2019; Pooch et al., 2019; Geirhos et al., 2020]. In addition, humans tend to be

---

Corresponding author(s): [lukas.muttenthaler@tu-berlin.de](mailto:lukas.muttenthaler@tu-berlin.de); [klaus-robert.mueller@tu-berlin.de](mailto:klaus-robert.mueller@tu-berlin.de), [lampinen@google.com](mailto:lampinen@google.com)

Confidential – Google DeepMind, do not share or forward externally.

© 2024 Google DeepMind. All rights reserved

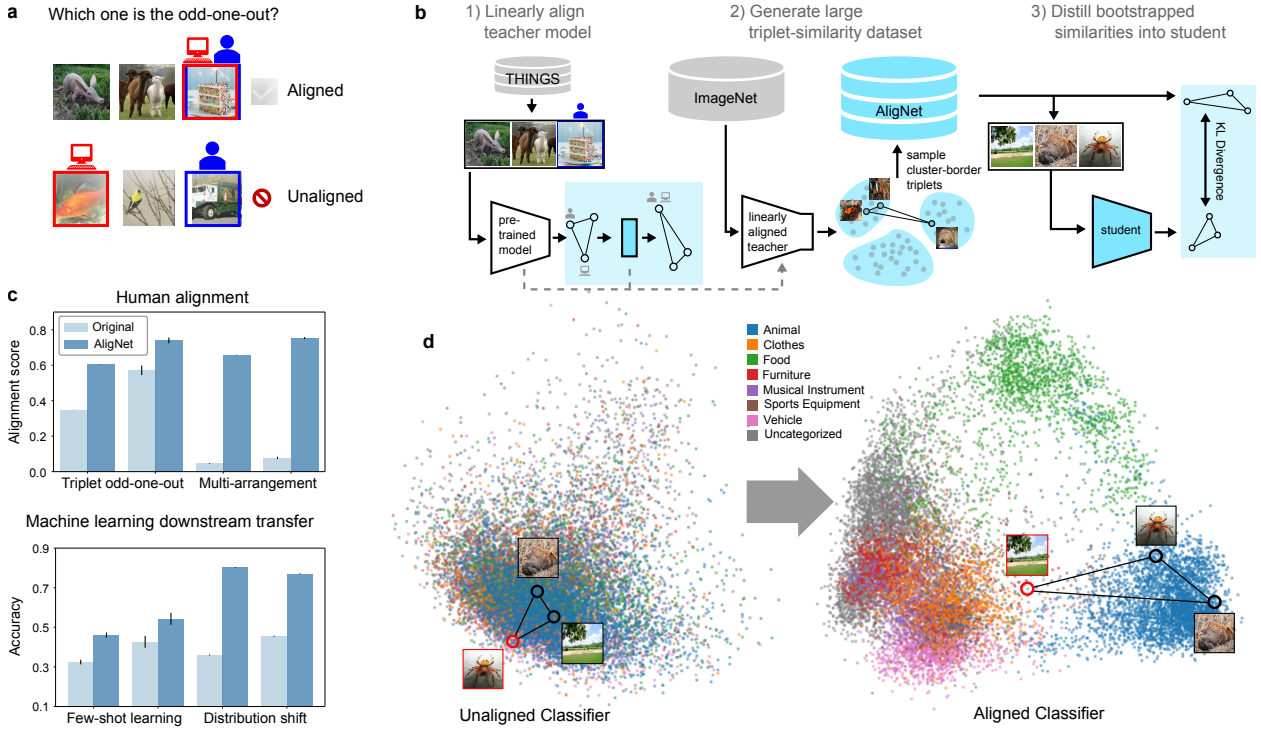


Figure 1 | A: An example of the triplet odd-one-out task where a human and a neural network model choose the same (top) and a different (bottom) odd-one-out image respectively. B: The different parts of the AligNet framework depicted from end to end. First, we develop a teacher model of human judgments using the THINGS dataset (first panel). Second, we apply this model to ImageNet and cluster its latent representations into semantically meaningful categories (second panel). This allows us to generate arbitrarily many similarity judgments. Third, the obtained human-like similarity structure information is distilled into a student vision foundation model using a novel loss function (third panel). C: Representative human alignment (top panel) and machine learning downstream (bottom panel) results show significant performance improvements of the aligned over the non-aligned version of the ViT-B classifier. D: 2D latent space projection for visualizing the change in the representations after alignment. While the representations of a standard ViT-B classifier model are unstructured and categories overlap, after alignment the representations are grouped into meaningful categories.

well-calibrated—for example, when they are asked to judge visual similarity [Roads and Mozer, 2017]—that is, humans’ (un)certainty tends to correlate with their (in)accuracy. AI systems, on the other hand, are often *overconfident* and show high certainty [Guo et al., 2017] even when their predictions are incorrect [Minderer et al., 2021]. Thus, many differences remain to be reconciled before we can ultimately achieve human-like artificial intelligence.

In this work, we highlight a key misalignment between humans and deep learning models that may underlie some of these differences: model representations tend to fail to capture the multi-level conceptual structure of human perception. Although model representations successfully encode the human-perceived similarity structure among entities that share *local* visual and semantic features (e.g., textures or colors of different breeds of dog), the *global* relationships between concepts that are more visually and semantically distinct (e.g., dogs and fish, which are both animate but are not visually similar at all) are modeled much less systematically. Human neural representations, however, are organized by global features like animacy [e.g., Kriegeskorte et al., 2008b; Cichy et al., 2019; Hebart et al., 2020], and at multiple finer scales that capture nuanced semantic relationships [Connolly et al., 2012; Cichy et al., 2019; King et al., 2019]. Could this lack of global organization in the representations of deep learning models across levels of the conceptual hierarchy contribute to

the aforementioned weaknesses of these models?

One key step to assessing—and addressing—this misalignment is to be able to systematically and reliably compare human and machine judgments, e.g., of similarity or categorical membership. Such comparisons are daunting, however, because of the substantial difference in data availability between the two sources. Human behavioral data is scarce because collecting representative samples is challenging and expensive [Cichy et al., 2019; King et al., 2019; Hebart et al., 2020, 2023]. The cost of getting (human) similarity judgments scales with the square of the number of images. For this reason, the largest human similarity-judgment datasets to date are several orders of magnitudes smaller than the datasets used to pretrain deep learning models. To build more accurate models of human perception, we propose a *novel framework that enables the simulation of arbitrarily large (albeit imperfect) human-like similarity judgment datasets for alignment via a teacher model* to render decisions of large neural network models more human-like.

We begin by using an affine transformation to align neural network model representations with human semantic judgments in triplet odd-one-out tasks [Muttenthaler et al., 2023a]. In doing so, we *regularize* the alignment to preserve the local representation structure of the models, and additionally leverage uncertainty measures over human responses to improve model calibration. This enables us to define a transformation toward more human-like representations of a state-of-the-art image/text vision foundation model (VFM). For the remainder of this paper, we use this aligned version of the VFM as a *surrogate model* for generating human similarity judgments. This approach is loosely analogous to the use of surrogate models for pseudo-labelling in semi-supervised classification learning [e.g. Lee, 2013]. With our surrogate model, we hypothesize that we can create a larger training dataset with multiple levels of conceptual granularity that will serve to provide cross-level constraints on human alignment.

To do so, we group the representations of the surrogate model into meaningful superordinate categories which we use to sample semantically meaningful triplets. Subsequently, we obtain odd-one-out responses from our surrogate model for all the triplets that we generate. This results in a large dataset of human-like triplet odd-one-out responses. We call this dataset *AligNet*. To transfer this carefully curated human-like similarity structure into a pretrained neural network foundation model, we introduce a new Kullback-Leibler divergence based objective function that facilitates the learning process. The different steps of the AligNet framework are visualized in Fig. 1B. While we use the ImageNet dataset [Russakovsky et al., 2014] because it is publicly available and widely used in the cognitive science and computer vision communities, our framework allows for different versions of AligNet to be created based on other image datasets, irrespective of whether the datasets are labelled.

To validate that AligNet can indeed help to increase the alignment between models and humans, we used crowd-sourcing to collect a novel evaluation dataset of human semantic judgments across multiple levels of abstraction that we call *Levels*. As anticipated, we find that models are worst at predicting human judgments that involve relationships among entities that have little visual or semantic overlap and are thus considered more *abstract*. We address this limitation by making models more human-aligned and correspondingly more robust. We demonstrate that the global or *coarse-grained* representational alignment instilled via AligNet—which we refer to as *soft-alignment*—improves model alignment with human judgments across a variety of visual similarity tasks. Additionally, we find that model uncertainty is better calibrated to human uncertainty. Moreover, soft-alignment substantially improves accuracy and robustness across many downstream machine learning tasks (see Fig. 1C), thus increasing the generalization capabilities of the model representations.

In summary, our work contributes to better understanding the key differences between artificial and natural intelligence. Moreover, our results illustrate a principle for aligning models and humans—focusing on the multi-resolution relational structure of human knowledge—that may be critical to

tackling the more general problem of achieving human-like artificial intelligence.

## 2. Results

*What is missing in modern learning systems to exhibit more human-like behavior?* We approach this question jointly from the perspectives of cognitive science and artificial intelligence. Specifically, our results below establish (1) a mathematical framework for aligning machine learning representations with human similarity judgments (see Sec. 2.1 and Sec. 4.1); and demonstrate that (2) our methodological framework, *soft-alignment*, indeed gives rise to systems with more human-like behavior in object similarity tasks by teaching models about the hierarchical structure of human conceptual knowledge (see Sec. 2.2). We demonstrate this using (i) human object similarity experiments using triplet odd-one-out or multi-arrangement tasks (see Sec. 2.2.1) and (ii) a new, carefully curated dataset, *Levels*, that allows us to systematically study the differences between human and deep learning model similarity spaces across three levels of knowledge abstraction (see Sec. 2.2.2). Moreover, we find that (3) soft-alignment leads to models that better reflect the hierarchical structure of human conceptual knowledge (see Sec. 2.3) and show that (4) soft-alignment improves generalization and robustness of models for a wide range of computer vision tasks (see Sec. 2.4).

### 2.1. Machine learning for alignment

To build models with more human-like behavior it is necessary to inject additional supervision about human behavior into the representations of foundation models. One way to achieve this is via an objective function that explicitly forces a model’s representation to inherit a human concept space [Muttenthaler et al., 2023a,b; Fu et al., 2023]. Previous work has shown that the objective function in addition to the (pre-)training data is the most central variable in the pursuit of human-like vision models [Muttenthaler et al., 2023a; Conwell et al., 2023].

We used the THINGS dataset [Hebart et al., 2020] — a behavioral dataset of human responses in a triplet odd-one-out task for object images — to build a *surrogate model* (denoted as *teacher*) that approximates a human object similarity space. This similarity space is determined by the human odd-one-out responses from which abstract human concepts can be inferred [Hebart et al., 2020; Muttenthaler et al., 2022]. To better match the human responses, we learned an affine transformation of the pretrained teacher model’s representation space of the form:  $\mathbf{x}' = \mathbf{W}\mathbf{x} + \mathbf{b}$ , where  $\mathbf{x} \in \mathbb{R}^p$  is the model’s latent representation for an object image in the data, and  $\mathbf{W}$  and  $\mathbf{b}$  are a learned transformation matrix and a bias vector respectively. The pairwise similarities of the teacher model between two object images  $i, j$  are modeled as the dot product between their corresponding transformed representations:  $S'_{i,j} := (\mathbf{W}\mathbf{x}_i + \mathbf{b})^\top (\mathbf{W}\mathbf{x}_j + \mathbf{b})$ . We obtained the affine transformation by maximizing the probability to select a human choice  $c := \{a, b\}$  given a triplet of object indices  $t := \{i, j, k\}$ , where  $c \subset t$ , and the corresponding object representations of the pretrained teacher model over  $n$  images:

$$\arg \min_{\mathbf{W}, \mathbf{b}} -\frac{1}{n} \sum_{s=1}^n \log p(c_s | t_s, \mathbf{S}') + \Gamma(\mathbf{W}),$$

where  $\Gamma(\mathbf{W})$  performs  $\ell_2$ -regularization of the transformation matrix  $\mathbf{W}$  toward the scaled identity matrix to preserve the local similarity structure of the original representation space (see Eq. 3 for more details about the type of regularization). We used stochastic gradient descent (SGD) to find the transformation variables  $\mathbf{W}$  and  $\mathbf{b}$ . See Sec. 4.1 and the Supplementary Material for more details about the optimization and how the affine transformation is learned.

After we found a transformation that best matches the human responses, we clustered the transformed teacher representations into meaningful superordinate categories (see Sec. 4.1 and the Supplementary Material). We used these clusters to sample triplets—two objects from one cluster and one from a different cluster—for generating a synthetic dataset of human-like triplet odd-one-out

responses. To transfer the structure of the pairwise similarity matrix of the teacher,  $S'$ , into a different student neural network  $f_{\theta^\dagger}$  (e.g., a Transformer-based VFM), we introduced a novel Kullback-Leibler divergence based objective function similar to Eq. 2 that facilitates the distillation process. This loss function is defined as

$$\mathcal{L}_{\text{alignet}}(S', S^\dagger) := \frac{1}{B} \sum_{s=1}^B \log \sigma \left( \left[ S'_{i,j}, S'_{i,j}, S'_{j,k} \right], \tau' \right)_s - \sigma \left( \left[ S'_{i,j}, S'_{i,j}, S'_{j,k} \right], \tau' \right)_s \log \sigma \left( \left[ S^\dagger_{i,j}, S^\dagger_{i,k}, S^\dagger_{j,k} \right], \tau^\dagger \right)_s,$$

where  $S'$  and  $S^\dagger$  are the pairwise similarity matrices of the teacher and the student representation spaces respectively,  $\sigma$  is a softmax function that transforms similarities into probabilities with temperature values  $\tau'$  and  $\tau^\dagger$  for the teacher and student respectively, and  $B$  is the total number of samples used for the similarity transfer. The final AligNet objective is defined as

$$\arg \min_{\theta^\dagger} \mathcal{L}_{\text{alignet}}(f_{\theta^\dagger}) + \lambda \|\theta^* - \theta^\dagger\|_2^2,$$

where  $\theta^*$  are the parameters of the pretrained student before fine-tuning by alignment and  $\theta^\dagger$  are the parameters of the fine-tuned student. The goal of the right-hand side of the equation is to preserve the fine-grained structure of the pretrained representation space as a function of  $\lambda$  which determines the strength of the regularization. See Fig. 1B for a visualization of the different steps in the AligNet framework. In the remainder of this manuscript, we refer to the approach of providing supervision regarding human object similarity via a surrogate teacher model as *soft-alignment*.

## 2.2. Toward human-like systems via a surrogate approach

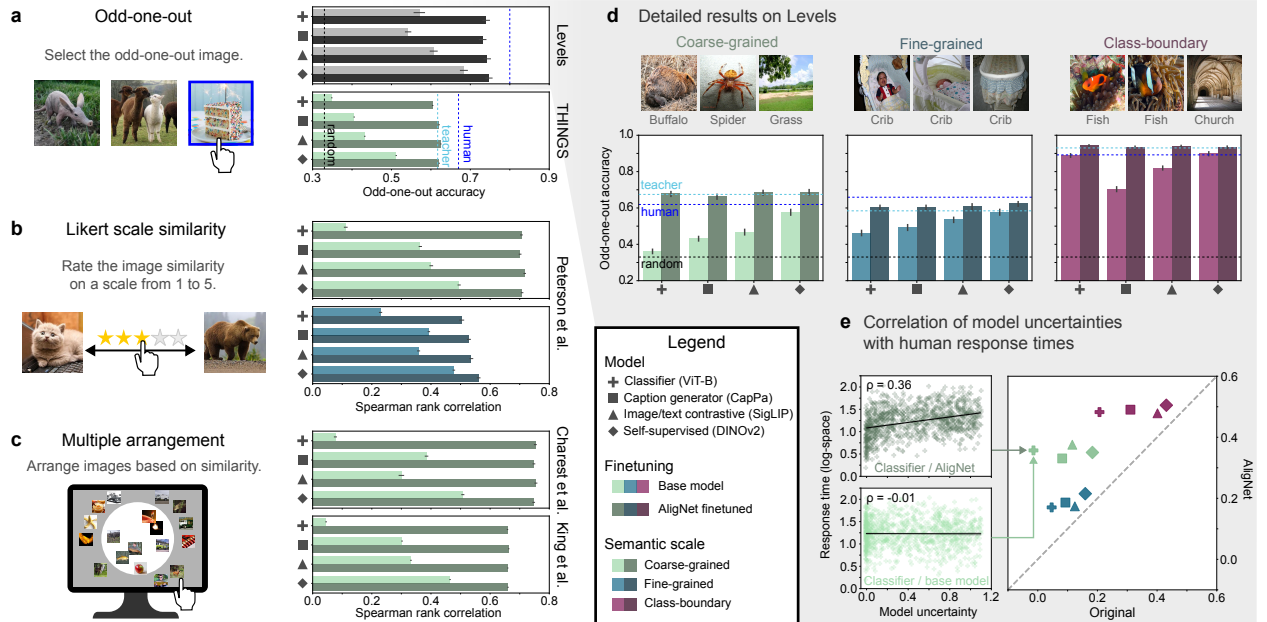


Figure 2 | Human alignment results. A: Odd-one-out accuracies on the THINGS dataset and performance averaged across all three levels of abstraction for Levels. B: Spearman rank correlations for the human response datasets from Peterson et al. [2018] for the coarse-grained various category and averaged across all fine-grained single domain categories. C: Spearman rank correlations for the multi-arrangement datasets from King et al. [2019] and Cichy et al. [2019] respectively. D: Odd-one-out accuracies on our datasets shown individually for the three levels of abstraction. E: Spearman rank correlation of model uncertainties and human response times. Model uncertainties are modeled as discrete Shannon entropy of the pairwise similarities in a triplet.

In the following, we demonstrate that soft-alignment gives rise to systems with more human-like behavior. We evaluated the alignment between human mental and neural network representations across a wide range of object similarity tasks using representational similarity analysis [RSA;

Kriegeskorte et al., 2008a] and by comparing responses in a triplet odd-one-out task [Muttenthaler et al., 2023a,b; Fu et al., 2023]. As in previous work [Cichy et al., 2019; King et al., 2019; Hebart et al., 2020; Muttenthaler et al., 2023a,b], we used the Spearman rank correlation coefficient to quantify the similarity of human and model representational similarity matrices (RSMs; for details see Sec. 4.2 or the Supplementary Material). As a measure of accuracy for the triplet odd-one-out task, we defined the degree of alignment as the fraction of triplets for which models selected the same odd-one-out choice as the human participants.

First, we validated that our surrogate model performs close to the human noise-ceiling of 66.67% for the THINGS triplet odd-one-out data [Hebart et al., 2020, 2023]. After applying the *Uncertainty Distillation* optimization (see Eq. 3) to the teacher model representations (see A.1.4 in the Supplementary Material), we observed a quantitative agreement with the human odd-one-out responses in 61.7% of all triplets in the THINGS data (see second dashed line in Fig. 2A). Second, given the triplet odd-one-out responses generated with our surrogate model, we found that after fine-tuning vision foundation models (VFs) on that data (see Sec. 2.1), all models showed significantly improved alignment with human judgments, irrespective of the pretraining task and the objective function used for training the base model, the cognitive similarity task, and the similarity metric (see Fig. 2A-C).

Notably, we observed relative increases in performance between 21.28 – 74.47% across a number of representative VFs trained on different tasks—image captioning, classification, self-supervised learning, image/text alignment—with different training objectives—supervised, unsupervised, self-supervised. Our findings generalize across various object similarity tasks that are commonly used in the cognitive sciences.

**Triplet odd-one-out task.** Models fine-tuned on AligNet achieved odd-one-out accuracies of 60.45% (ViT-B) – 62.54% (SigLIP ViT-B) of which 62.54% is the best alignment score of a neural network model on the THINGS dataset to date [c.f. Muttenthaler et al., 2023a,b]. In contrast, the base model representations achieved odd-one-out accuracies of 34.87% (ViT-B) – 51.21% (DINOv2 ViT-B). The odd-one-out accuracy of ViT-B increased substantially from 34.87% to 60.45%. This is a relative increase in performance of 73.35%. All performance increases are statistically significant at  $\alpha = 0.05$ .

It is not surprising that AligNet fine-tuning significantly improved the alignment of models with the THINGS triplet odd-one-out choices because the affine transformation that is part of the distillation process was learned on that data (see Sec. 2.1 and Sec. 4.1). Thus, we validated whether models fine-tuned on AligNet generalize to other human similarity judgment datasets beyond the THINGS triplet dataset.

**Other object similarity tasks.** We performed our evaluation on the same human similarity judgment datasets that were analyzed in Muttenthaler et al. [2023b]. The human similarity judgments were collected by either asking participants to arrange natural object images from different categories on a computer screen [Cichy et al., 2019; King et al., 2019] or rate pairwise similarities on an ordinal Likert scale [Peterson et al., 2018]. See the Supplementary Material for more details about the datasets and how they were collected.

We found that AligNet fine-tuned models are substantially better-aligned with human similarity judgments than their base models and even better than an affine transformation learned on the THINGS dataset (see the Supplementary Material for the latter finding). This observation holds irrespective of the similarity task—multi-arrangement [Cichy et al., 2019; King et al., 2019] or Likert-scale pairwise similarity ratings [Peterson et al., 2016, 2018]—that was used to infer object similarity from the human subjects. See Fig. 2B,C for how much AligNet fine-tuning improved the degree of alignment upon their base model representations, measured as Spearman rank correlation between the upper triangulars of model and human RSMs (see Sec. 4.2 for how RSMs are obtained).

While the base model representations achieve Spearman rank correlation coefficients of  $\rho = 0.045 - 0.508$  and  $\rho = 0.223 - 0.477$  with the human responses for coarse-grained and fine-grained object similarity respectively, AligNet models showed a statistically significant improvement in the correlation coefficients and achieved Spearman rank correlations of  $\rho = 0.655 - 0.760$ ,  $p < 0.001$  for coarse-grained and  $\rho = 0.499 - 0.561$ ,  $p < 0.001$  for fine-grained object similarity, depending on the dataset (Peterson et al. [2016, 2018]:  $\rho = 0.670 - 0.717$ ,  $p < 0.001$  for coarse,  $\rho = 0.499 - 0.561$ ,  $p < 0.001$  for fine; Cichy et al. [2019]:  $\rho = 0.747 - 0.760$ ,  $p < 0.001$ ; King et al. [2019]:  $\rho = 0.655 - 0.666$ ,  $p < 0.001$ ). The improvements for the classifier are particularly striking and range from a 6.3 fold increase in Spearman rank correlation coefficient for Peterson et al. [2016, 2018] to a 14.47 fold increase for King et al. [2019].

### 2.2.1. The Levels dataset of human similarity judgments

To systematically validate that *soft-alignment yields model representations that reflect the hierarchical structure of human conceptual knowledge*, we collected a new multi-resolution similarity judgment dataset called *Levels*. This dataset was based on the triplet odd-one-out task and included judgments on three different types of triplets: *global coarse-grained semantic*, which require deciding on the odd-one-out in broadly different categories; *local fine-grained semantic*, involving discerning subtle distinctions within the same category; and *class-boundary*, testing the capacity to identify category boundaries. For details about *Levels* see Sec. 4.3.

**Descriptive statistics for human response times and uncertainty measures.** We examined the human response time (RT) differences across the three abstraction settings as an indicator of the cognitive processing demands required to select the odd-one-out (see Fig. 5A). As expected, responses were fastest in the class-boundary triplets ( $Mdn = 2.05$  s,  $SE = 0.01$ ), which probed decisions with relatively low ambiguity. RTs for fine-grained semantic triplets were significantly longer ( $Mdn = 3.01$  s,  $SE = 0.01$ ;  $t(447) = 48.784$ ,  $p < 0.001$ ), and the longest RTs were observed for the coarse-grained semantic triplets ( $Mdn = 3.25$  s,  $SE = 0.01$ ;  $t(447) = 15.036$ ,  $p < 0.001$  compared to fine-grained). An explanation for the longer RTs in the latter conditions can be that these triplets involved complex, multi-level decisions where participants may have weighed multiple factors (e.g., perceptual and/or semantic) to arrive at choice. This contrasts with the clear semantic boundaries that could be used to identify the odd-one-out in class-boundary triplets. Consistent with the RT results, we also found higher levels of cross-participant agreement (see Fig. 5C) in the class boundary condition compared to both the coarse-grained semantic and the fine-grained semantic conditions.

We used participants' RTs as a proxy of their decision uncertainty. The human RTs for the individual triplets correlated positively with the level of cross-participant disagreement on those triplets (see Supplementary Material Sec. A.3 and Fig. 5B), in each of the abstraction settings (coarse-grained semantic:  $r = 0.325$ ,  $p < 0.001$ ; fine-grained semantic:  $r = 0.364$ ,  $p < 0.001$ ; class-boundary:  $r = 0.443$ ,  $p < 0.001$ ), suggesting that human RTs provided a reasonable approximation of decision uncertainty for model-to-human comparison.

**Human-to-human alignment.** We computed the human noise ceiling for each abstraction setting in *Levels* using a Leave-One-Out (LOO) cross-validation approach. In LOO, the agreement level for a triplet is computed as the average match-rate between a held-out participant's response and the majority response of the remaining population. Thus, for a triplet with five responses, one response is held out and the remaining four comprise the population. The human-to-human reliability score is then calculated as the average agreement level across all triplets in the dataset.

### 2.2.2. Alignment at multiple levels of abstraction

The Levels dataset allows to systematically study discrepancies between human and deep learning model decisions across different levels of complexity. Here, we demonstrate that soft-alignment can reduce those discrepancies: it makes it possible to incorporate the hierarchical structure of human conceptual knowledge into foundation model representations.

**Global coarse-grained.** We found the largest differences between model and human similarity judgments before AligNet fine-tuning were present for global coarse-grained semantics. The base models achieved low odd-one-out accuracies of 36.09% (ViT-B) – 57.38% (DINOv2 ViT-B). Soft-alignment significantly improved the alignment between human and model responses to the extent that all models performed above the human-to-human reliability score of 61.92% (see Fig. 2D, leftmost column) with odd-one-out accuracies of 65.70% (DINOv1 ViT-B) – 68.56% (DINOv2 ViT-B). The relative improvements in performance ranged from 19.48% (DINOv2 ViT-B) – 93.51% (ViT-L).

**Local fine-grained.** The performance of most base models (except for DINOv1 ViT-B) did not strongly correspond to human responses for fine-grained semantics either and, thus, model performances were far from the human noise ceiling of 65.92%. Prior to fine-tuning, models achieved poor alignment scores of 46.04% (ViT-B) – 57.72% (DINOv2 ViT-B), except for DINOv1 ViT-B which performed (62.92%) significantly better than any other model in that setting (see Tab. 3 in the Supplementary Material). AligNet fine-tuning improved this mismatch to some degree but not as substantially as it did for the coarse-grained abstraction level. AligNet models achieved odd-one-out accuracies of 58.93 (ViT-S) – 62.92% (DINOv1 ViT-B). This is equal to a relative increase in performance of 7.84% (DINOv2 ViT-B) - 46.03% (ViT-L) (see Fig. 2D, middle column).

**Class-boundary.** Supervised classifiers and image/text contrastive models performed close to the noise ceiling for class-boundary triplets prior to any fine-tuning. Their odd-one-out accuracies ranged from 81.96% (SigLIP ViT-B) to 93.67% (ViT-L) (see Tab. 3). However, the caption generator model (CapPa) often responded quite differently from humans in that setting and achieved a low odd-one-out accuracy score of 70.37%. AligNet fine-tuning changed the representation spaces of all models that we considered to be equally well aligned. There are small differences between the models but they are not statistically significant. Surprisingly, AligNet models' odd-one-out accuracies were higher than the human noise ceiling of 89.21% (see Fig. 2D, rightmost column) with the best model achieving an alignment score of 93.24% (ViT-L). This means that the responses of AligNet models were more similar to the average human responses—since each triplet response is the majority response of the subject population—than the level of agreement among the human subjects themselves. The variance in accuracy among AligNet models was much smaller compared to the other two abstraction settings, with odd-one-out accuracies of 93.09% – 94.24%. The relative increases in performance for this setting were between 0.62% (ViT-L) - 32.29% (CapPa ViT-B). For more details about model performances on Levels see Tab. 3 in the Supplementary Material.

**Human alignment depends on the abstraction level.** We found that the best model before soft-alignment at a particular abstraction level was often not the best model after soft-alignment. While DINOv2 was the best aligned model before AligNet fine-tuning for the fine-grained (57.38%) and coarse-grained (57.72%) abstraction settings (see Tab. 3 in the Supplementary Material), it remained the best aligned model only for the fine-grained setting (62.24%) but did not improve as significantly as the other models for the coarse-grained (relative improvement of 18.78%) and class-boundary settings (relative improvement of 4.13%). On the other hand, ViT-L was the worst-aligned model before fine-tuning for the coarse-grained setting (35.45%), but after AligNet fine-tuning, it became the best-aligned model, achieving the highest odd-one-out accuracy (68.60%) across all models. The relative improvement in performance was 93.51%. In addition, ViT-L was both the best aligned model before (93.67%) and after (94.24%) AligNet fine-tuning for the class-boundary setting (both scores

are higher than the human reliability score of 89.21%).

We observed a similar phenomenon for the coarse- and fine-grained human responses datasets of [Peterson et al. \[2016, 2018\]](#). DINOv2 showed the highest Spearman rank correlation coefficient with the human similarity judgments prior to any fine-tuning for both abstraction levels but remained the best aligned model only for the fine-grained datasets after fine-tuning (see Tab. 2 in the Supplementary Material for details). This suggests that DINOv2 fine-tuned on AligNet best captured fine-grained human semantic structure whereas image/text contrastive and supervised models best reflected coarse-grained and class-boundary semantic structure respectively after the fine-tuning process.

**Model uncertainties correspond to human latencies after soft-alignment.** In addition to discrete odd-one-out choices, we collected (continuous) human response times (RTs) for each participant and triplet. Human response latencies are indicative of the uncertainty of a participant’s choice (see Sec. 2.2.1). Thus, here we use them as a proxy of the participants’ uncertainty [[Ratcliff, 1978](#); [Kiani et al., 2014](#)]. We measured the uncertainty of model responses as the discrete Shannon entropy of the three pairwise similarities within each triplet. The triplet uncertainties of the base models were not correlated with the human latencies for the coarse-grained ( $\rho = -0.014 - 0.184$ ) and fine-grained settings ( $\rho = 0.047 - 0.160$ ) and showed a medium positive correlation for the class boundary setting ( $\rho = 0.208 - 0.432$ ). After soft-alignment, the correlations substantially increased for all models and abstraction settings (see Fig. 2E). The increase in correlation was particularly striking for the coarse-grained abstraction level: AligNet models showed weak positive correlations for the fine-grained ( $\rho = 0.171 - 0.216$ ), medium positive correlations for the coarse-grained ( $\rho = 0.331 - 0.376$ ), and strong positive correlations for the class-boundary setting ( $\rho = 0.479 - 0.506$ ). Correlations were measured as Spearman rank correlation coefficients.

### 2.3. Aligned models reflect the conceptual hierarchy

*How do the model representations change after soft-alignment?* In Fig. 3 we show that while the model representations are dissimilar before alignment (especially those trained on classification tasks), they become much more similar to each other after soft-alignment. (See Sec. 4.4 for details.)

One reason for this convergence is that the models align better with the human semantic category hierarchy [cf. [Rosch et al., 1976](#)]. The organization during alignment is driven by two factors: first, as shown in Section 2.2, the labels generated by the model will tend to reflect human judgments and uncertainty, especially in the relationships at more abstract levels of the category hierarchy. However, the *clustering* process that we use to sample the triplets *also* reflects this hierarchical structure. In particular, it tends to produce triplets where the similar pair of images come from the same subordinate- or basic-level category, while the odd-one-out comes from either a different basic-level or superordinate category (Fig. 3C). Thus, our soft-alignment procedure embeds the global structure in multiple ways: both in clustering and labeling.

The impact of this hierarchical alignment is that the relationships between representations of different images change depending on the semantic relationship between them. The representations of images from the same basic category tend to move much closer together, those of images from the same superordinate category tend to move somewhat closer together, and those from different superordinate categories tend to move farther apart. Thus, the alignment procedure drives model representations to reorganize according to the global structure of human knowledge, as we intended. (Results in Fig. 3D-E are for ViT-B; for other models see SI B.3.2.)

As an illustrative example, in a standard ViT-B classifier the representations of lizards are initially closer to those of some plants and fruits due their similarity in texture, color, or background conditions; after alignment, they are naturally more similar to the representations of other animals and more distant from those of other, unrelated superordinate categories (see Figure 1D). This organization

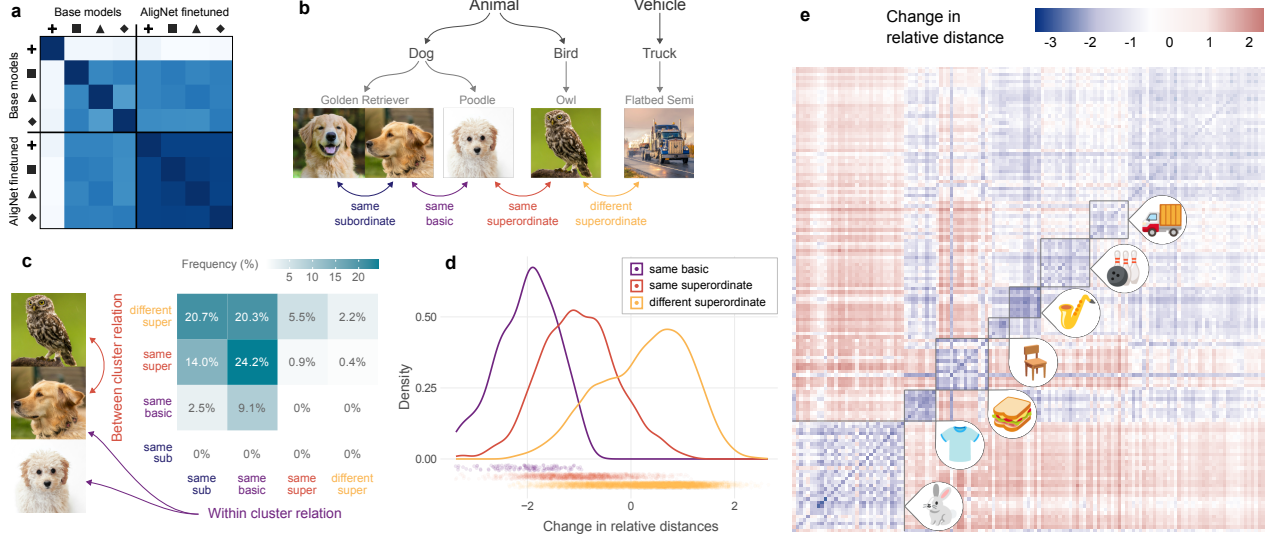


Figure 3 | Aligned models reflect the semantic hierarchy. **A:** Before alignment, models trained with different losses have dissimilar representation structures—particularly those trained for supervised classification. After alignment, however, model representation structures are much more similar to each other. **B:** To understand the alignment, we study how the models’ representations change across the semantic hierarchy, from relations between images within the same subordinate category to relations across superordinate categories. **C:** The cluster-driven triplet sampling tends to produce triplets where two images have a closer relation than the third. **D:** The result is that the relations between image representations change following the semantic hierarchy—images from the same basic or superordinate category tend to move closer together, while those from different superordinate categories move farther apart. **E:** Visualizing the distance changes in more detail, with some superordinate categories boxed on the diagonal and labelled with icons on the axes. (Panels D-E are for the representations of ViT-B.)

will yield better generalization when lizards are anomalous among a category of fruits, or when a lizard image is used as one of the examples depicting a more abstract category like animals.

#### 2.4. Alignment improves generalization and out-of-distribution robustness

*What are the consequences of more human-like structured model representations induced by soft-alignment for machine learning tasks?* To address this question, we investigated how alignment alters generalization and out-of-distribution robustness of foundation models across different machine learning downstream tasks.

To obtain a measure that systematically evaluates the quality of the models’ representations, we froze the weights of the neural network model and trained a linear classifier on top of the model’s image representations rather than training/fine-tuning the entire model. A key question for any real-world application is how well a model generalizes to new settings, tasks, and objects. Hence, we studied (a) one-shot classification tasks, (b) distribution shift and (c) out-of-distribution robustness.

**One-shot classification.** *One-shot classification tasks* are among the hardest scenarios for testing generalization: the objective is to classify images given only a single labelled example per class. In Fig. 4 we show one-shot performance of all models before and after AligNet finetuning on a ten image-classification datasets from a wide variety of domains, such as fine-grained birds classification [Birds; Welinder et al., 2010], land use classification from satellite imagery [UC Merced; Yang and Newsam, 2010], and colorectal cancer histology [Colon; Kather et al., 2016]. While for eight combinations of model and dataset, we find a small decrease in performance, the majority of cases (32) show an improvement, sometimes by a substantial margin (e.g. accuracy of DINoV2 on Pets shows a 2.7 fold increase). Overall our alignment framework increased the generalization performance on these

task significantly ( $p < 0.05$ ). These results corroborate the hypothesis that a good coarse-level (re-)structuring of the representation space supports generalization in general and especially for tasks where little labelled data is available.

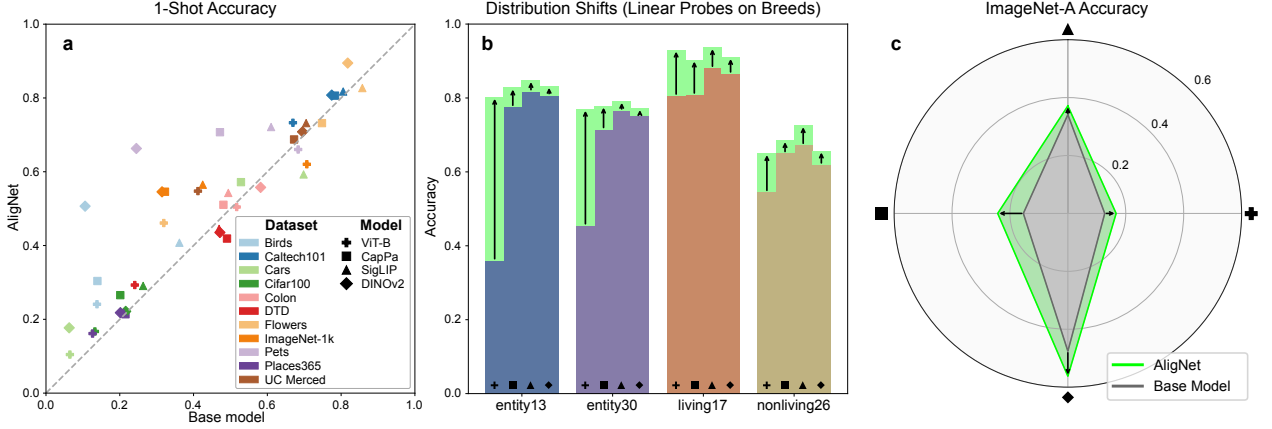


Figure 4 | Machine learning downstream results. We evaluated how AligNet finetuning affected the downstream task performances of various pre-trained VFMIs using liner probing. **A:** 1-shot accuracy before (x-axis) vs. after (y-axis) AligNet finetuning on various image datasets. **B:** Accuracy improvements on the four BREEDS distribution shift benchmark datasets. **C:** Accuracy improvements on the ImageNet-A dataset that evaluates model robustness.

**Distribution shift.** A long-standing problem of applying machine learning algorithms in practice is distribution shift and domain adaptation [cf. [Sugiyama et al., 2007](#); [Sugiyama and Kawanabe, 2012](#); [Farahani et al., 2021](#)]: as machine learning systems are deployed, the data they were originally trained on often differs in subtle ways from the data they are being applied to. Models tend to fail in unexpected ways when the data they should predict has a different distribution than the training data.

To measure if the global category structure induced by fine-tuning on AligNet helps to address such distributional shifts, we use the BREEDS benchmarks [[Santurkar et al., 2020](#)]. These were specifically designed explore generalization under input distributions shifts, by constructing datasets where the samples from training and test are sampled from different sub-populations. Fig. 4B shows the result of training a linear readout layer on the four BREEDS training sets, and evaluating them on the corresponding test-sets. AligNet fine-tuning consistently improves performance across all benchmarks and models types. The image classifier (ViT-B) benefits the most with a more than twofold increase for the ‘entity13’ benchmark.

**Model robustness.** A further benefit of alignment is that it has a positive influence on the robustness of a model. [Hendrycks et al. \[2021b\]](#) collected a challenging dataset of natural images that are adversarial, in the sense that neural networks tend to consistently misclassify them, while they are obvious for humans. Again, we find that AligNet fine-tuning improves the accuracy across all VFMs that we investigate (cf. Fig. 4C); specifically, we observe improvements of up to 9.5 percentage points, which corresponds to a 1.6 fold improvement for the CapPa model.

Taken together, all of these results corroborate that aligning human and neural network model representations helps to generalize better, transfer to new tasks and data, and enhances model robustness. In other words, alignment is helpful for practically improving deep learning.

### 3. Discussion

The differences between natural intelligence and the capabilities of neural networks are the subject of long-standing debates [Fodor and Pylyshyn, 1988; Lake et al., 2017]. Despite the dramatic progress in AI of the past decade, these discussions persist, because even the most successful deep learning systems seem to fail in non-human-like ways [Lake et al., 2015; Lapuschkin et al., 2019; Geirhos et al., 2020; Thrush et al., 2022; Muttenthaler et al., 2023a; Lake and Baroni, 2023; Puatruauean et al., 2023].

In this work, we have highlighted—and addressed—a key deficiency in a broad class of vision foundation models: their representations do not adequately represent the multi-level conceptual structure of semantic knowledge that is natural to humans (see Sec. 2.2). We demonstrate this deficiency by collecting a new dataset of stratified human similarity judgments across multiple levels of abstraction—which we call *Levels* (see Sec. 2.2.2). To address this deficiency, we established a methodological framework for aligning deep learning models with human similarity judgments to build systems that exhibit more human-like behavior (see Sec. 2.1). By bootstrapping from a relatively small quantity of human data, we develop a surrogate neural network model of human object similarity judgments. Analogous to prior work on semi-supervised classification [e.g. Lee, 2013; Grandvalet and Bengio, 2004], we use this surrogate model to label a larger dataset for which we do not have human judgments. Specifically, we propose a cluster-based triplet-sampling technique for ImageNet images, which we then label with *human-like* odd-one-out responses from our surrogate model to create a large new synthetic dataset called *AligNet*.

We fine-tuned a wide range of vision foundation models on AligNet, using a novel KL-divergence-based objective function for injecting human-like similarity structure (i.e., hierarchical conceptual knowledge) into the models. We systematically demonstrate that using this framework yields significantly *increased alignment* to human judgments on many cognitive science tasks (see Sec. 2.2), as well as *better performance* on various representative machine learning tasks (see Sec. 2.4). In other words, *soft-alignment* helps to alleviate the brittleness of machine learning models under changing environments. Moreover, our results illustrate how the broader paradigm of studying representational alignment [Kriegeskorte et al., 2008a; Sucholutsky et al., 2023] can not only yield *insights* by measuring *how systems differ*, but can be leveraged to actively align model representations with human conceptual hierarchies (see Sec. 2.3) to *improve the models’ generalization and robustness*.

These results contribute to the long-standing debate over whether neural network models can capture the full range of human intelligence [Fodor and Pylyshyn, 1988; Marcus, 1998; McClelland et al., 2010; Holyoak and Hummel, 2014; Tenenbaum et al., 2011; Lake et al., 2017]. In particular, relational understanding is thought to be a distinguishing feature of human intelligence [Gentner, 2003; Waltz et al., 1999; Penn et al., 2008], and one relevant line of critique has argued that neural networks lack the capability to appropriately represent abstract relations like same and different [Marcus, 1998; Holyoak and Hummel, 2014], or to organize knowledge into hierarchies of concepts and their relations [Tenenbaum et al., 2011]. While some aspects of these critiques have been refuted in simpler synthetic settings [e.g. Geiger et al., 2023], similar criticisms persist for modern foundation models—including the specific claim that empirical weaknesses in vision models make them deeply flawed as cognitive models [Bowers et al., 2022]. Our results show that, while standard objectives do not adequately capture the hierarchy of relations within and across categories, these relations can be distilled into the models—and this procedure substantially improves the models’ resilience under the kinds of distribution shifts that have concerned some prior critiques.

Although in this work we focused on the visual domain, similar global misalignments likely arise in other areas of machine learning research. For instance, in natural language processing, models are similarly trained with objectives that focus on distinguishing between close matches (e.g., prediction

objectives that primarily distinguish words that occur in the current context from those that would occur in slightly different contexts, rather than considering their relations to less probable concepts). Applying alignment techniques to natural language processing may therefore analogously help to better capture the global structure of semantic and syntactic relationships among language inputs that these objectives miss.

Reconciling global and local structures is a long-standing problem across the natural sciences. For example, the inherent complexities of molecules and materials need both short-range (local) and long-range (global) components. The Schroedinger equation accurately describes this intricate interplay. Thus, modelling in quantum mechanics can use the laws of physics as inductive biases (see e.g. physics informed learning). Constraining [e.g., [Chmiela et al., 2017, 2018](#); [Schmitz et al., 2022](#)] or regularizing [e.g., [Karniadakis et al., 2021](#)] models using physical priors/laws can explicitly include such global and local dependency components.

In contrast, the fields of vision and language processing do not offer equations that enable the direct access to local and global relationships between objects, scenes, or words. Therefore, in the AlignNet framework we propose to use human knowledge as a *regularizer* to achieve the desired representations. A more general insight is that the implicit knowledge of humans can be made readily accessible to learning systems via soft-alignment. Thus, learning systems become more human-like *because* in addition to local information they can now reflect global relationships. We hypothesize that this approach could also be applied to other domains where human judgements of global relations are accessible, but equations are not.

We remark that AI systems have been successfully adopted in many areas across the sciences and industries. However, these deployments lead to many *practical* [[Paley et al., 2023](#)] and *conceptual* [[Amodei et al., 2016](#)] concerns such as trustworthiness, biases, safety issues, and miscalibration. It is therefore increasingly important to identify the reasons why these systems occasionally fail (e.g., global misalignment, non-robustness, spurious correlations, or shortcut learning) and how to alleviate these failures. Our work advances the understanding of the deficiencies of a major class of current systems, and simultaneously shows a viable path for ameliorating these deficiencies by alignment with human judgments.

In order to most effectively build on this work, there are a number of limitations that could be addressed in future efforts. First, the neural network models we used neither account for context in similarity judgments nor higher-order relations. These factors could possibly be accounted for with more complex models, such as contemporary vision-language models [e.g. [Team et al., 2023](#); [OpenAI et al., 2023](#)], with which performance and alignment across different contexts could be readily explored. Additionally, in this work we generally treat the human representation as if it were unique—stressing the intrinsic uncertainty across individuals. However, human representations may vary systematically across individuals, cultures, and so on. Exploring this dimension of variation in human judgments would be an important topic for future investigation. Finally, human judgment is full of flaws, intrinsic contradictions and discrepancies. Given these issues, perfect alignment to human performance may not always be desirable for a technical system. Thus, future work could explore how to best learn from human knowledge without adopting human imperfections.

In summary, we have provided an initial blueprint of how to distill global, human-like similarity structures into the representations of modern deep neural networks. We demonstrated a viable path toward a *best-of-both-worlds representation* that is both more consistent with human cognition and more practically useful in the machine learning domain, paving the way toward more robust, interpretable, and human-like artificial intelligence systems. We hope that our work will inspire more general approaches to (softly) aligning models by distilling priors from human cognition into their representations.

## 4. Methods summary

### 4.1. AligNet

**THINGS dataset objects.** Similar to [Muttenthaler et al. \[2023a,b\]](#), we use the THINGS triplet odd-one-out dataset [\[Hebart et al., 2020\]](#) for learning an affine transformation into a (global) human object similarity space. The THINGS dataset can formally be defined as  $\mathcal{D} := (\{a_s, b_s\} \mid \{i_s, j_s, k_s\})_{s=1}^n$  which denotes a dataset of  $n$  object triplets and corresponding human odd-one-out responses, where  $\{a, b\} \subset \{i, j, k\}$  and  $\{a, b\}$  is the object pair that was chosen by a human participant to have the highest similarity. Let  $X \in \mathbb{R}^{m \times p}$  be the teacher model representations for the  $m = 1854$  objects in the THINGS dataset. Note that each category in the THINGS dataset is represented by one object image. From  $X$  we can construct a similarity matrix for all object pairs  $S := XX^\top \in \mathbb{R}^{m \times m}$ , where  $S_{ij} = x_i^\top x_j$  is the representational similarity for objects  $i, j$ .

**Linear transformation.** Our goal is to learn an affine transformation into the THINGS human object similarity space of the form:  $x' = Wx + b$ . Here,  $W \in \mathbb{R}^{p \times p}$  is a learned transformation matrix,  $b \in \mathbb{R}^p$  is a bias, and  $x \in \mathbb{R}^p$  is the neural network representation for a single object image in the THINGS dataset. We learn the affine transformation for the representation of the image encoder space of the SigLIP-So400m teacher model (see Sec. [A.1.4](#) for details about the teacher model). Using this affine transformation, an entry in the pairwise similarity matrix  $S'$ —which represents the similarity between two object images  $i, j$ —can now be written as  $S'_{i,j} := (Wx_i + b)^\top (Wx_j + b)$ .

**Uncertainty distillation.** We mainly follow the optimization process introduced in [Muttenthaler et al. \[2023b\]](#). However, we modify their approach by injecting uncertainty measures about human odd-one-out responses into the representation space of the teacher, using a recent approximate Bayesian inference method for learning object concepts from human behavior [\[Muttenthaler et al., 2022\]](#). Thus, we replace the negative log-likelihood of the discrete human odd-one-out choices—which we refer to as *hard-alignment*—with the negative log-likelihood of the probabilities for the pairwise triplet similarities obtained from the Bayesian inference model—referred to as *soft-alignment*. Hard-alignment is defined as,

$$\mathcal{L}_{\text{hard-align}}(S') := -\frac{1}{n} \sum_{s=1}^n \log \underbrace{q(\{a_s, b_s\} \mid \{i_s, j_s, k_s\}, S')}_\text{odd-one-out prediction}, \quad (1)$$

where the affine transformation of the teacher’s representation space is optimized to match the (discrete) human responses. In contrast, soft-alignment gives the following KL divergence between the human uncertainties  $p^*$  and the teacher model probabilities  $q$  obtained from applying a softmax function to the pairwise similarities of  $S$ ,

$$\mathcal{L}_{\text{soft-align}}(S') := \frac{1}{n} \sum_{s=1}^n \log \underbrace{p_s^*(\{i_s, j_s, k_s\})}_\text{human uncertainty} - \underbrace{p_s^*(\{i_s, j_s, k_s\}) \log q_s(\{i_s, j_s, k_s\}, S')}_\text{cross-entropy}, \quad (2)$$

The final objective for learning the *uncertainty distillation* (UD) transformation is defined as

$$\arg \min_{W, b} \underbrace{\mathcal{L}_{\text{soft-align}}(X, W, b)}_\text{soft alignment} + \lambda \left\| W - \left( \sum_{j=1}^p W_{jj}/p \right) I \right\|_\text{F}^2, \quad (3)$$

where  $I \in \mathbb{R}^{p \times p}$  is the identity matrix. The right-hand side of the above objective is an  $\ell_2$ -regularization whose aim is to preserve the nearest neighbor information (or equivalently, the local similarity structure) of the pretrained representations while learning an affine transformation into the THINGS human object similarity space. The above equation is minimized using standard SGD.

**Superordinate clusters.** We embed the ImageNet train set in the transformed representation space of the teacher and cluster the representations into superordinate categories using  $k$ -Means clustering. We find the optimal number of clusters  $k$  using the Elbow criterion. We use the clusters for generating triplets of distinct ImageNet images by always sampling two images from the same cluster and one image from a different cluster. For all triplets that we generate we identify their odd-one-out choice using the representations of the surrogate teacher model.

**Human-like responses.** The responses of the surrogate model simulate a dataset of human-like triplet odd-one-out responses. In addition to the discrete odd-one-out choices, the dataset includes the exact relationships among all pairwise similarities in a triplet obtained from the probability space of the teacher model. Thus, we now have access to soft choices.

**AligNet objective.** To distill the pairwise similarity structure of the teacher into a different student network, we introduce a novel Kullback-Leibler divergence based objective function similar to Eq. 2 that facilitates the distillation process. This loss function is defined as

$$\mathcal{L}_{\text{alignet}}(\mathbf{S}', \mathbf{S}^\dagger) := \frac{1}{B} \sum_{s=1}^B \log \sigma \left( \left[ S'_{i,j}, S'_{i,j}, S'_{j,k} \right], \tau' \right)_s - \sigma \left( \left[ S'_{i,j}, S'_{i,j}, S'_{j,k} \right], \tau' \right)_s \log \sigma \left( \left[ S^\dagger_{i,j}, S^\dagger_{i,k}, S^\dagger_{j,k} \right], \tau^\dagger \right)_s,$$

where  $\mathbf{S}'$  and  $\mathbf{S}^\dagger$  are the pairwise similarity matrices of the teacher and the student representation spaces respectively,  $B$  is the number of image triplets in a batch,  $\sigma$  is a softmax function that transforms the similarities into probabilities, and  $\tau'$  and  $\tau^\dagger$  are temperature values for the teacher and student that we find via grid search. The final AligNet objective is defined as

$$\arg \min_{\theta^\dagger} \mathcal{L}_{\text{alignet}}(f_{\theta^\dagger}) + \lambda \|\theta^* - \theta^\dagger\|_2^2,$$

where  $\theta^*$  are the parameters of the pretrained student before fine-tuning and  $\theta^\dagger$  are the parameters of the fine-tuned student. The right-hand side is similar to the  $\ell_2$ -regularization employed for learning the UD transformation. It tries to preserve the structure of the pretrained representation space as a function of  $\lambda$  which determines the strength of the regularization.

## 4.2. Representational Similarity Analysis

Representational Similarity Analysis (RSA) is a well-established method for comparing neural network representations—extracted from an arbitrary layer of the model—to representations obtained from human behavior [Kriegeskorte et al., 2008a]. In RSA, one first obtains representational similarity matrices (RSMs) for the human behavioral judgments and for the neural network representations (more specific details can be found in the Supplementary Material). These RSMs measure the similarity between pairs of examples according to each source. As in previous work [Cichy et al., 2019; King et al., 2019; Hebart et al., 2020; Muttenthaler et al., 2023a,b], we flatten the upper triangular of human and model RSMs respectively and quantify their similarities using the Spearman rank correlation coefficient. In contrast to the Pearson correlation coefficient, the Spearman rank correlation is scale-invariant and thus better suited to measure similarities of judgments obtained from different sources.

## 4.3. Levels

We collected a new multi-level similarity judgment dataset from  $N = 473$  human participants, which we named *Levels*. This dataset is based on the triplet odd-one-out task and included judgments on three different types of triplets: *coarse-grained semantic*, which require deciding on the odd-one-out in broadly different categories; *fine-grained semantic*, which involved discerning subtle distinctions within the same category; and *class-boundary*, which tested for the capacity to identify category

boundaries. When predominantly one image (e.g.,  $i$ ) was selected to be the odd-one-out across multiple participants, it indicated that the other two images (e.g.,  $j$  and  $k$ ), which were not selected, were closer to each other in the participants' concept space than either was to the odd-one-out (see Sec. 4.3 and the Supplementary Material for details about the data collection). This dataset allowed us to evaluate whether neural network models respond similarly as humans for the same set of stimuli on various levels of abstraction, and to examine the extent to which the models capture the inherent uncertainty in human judgments, as inferred from response latencies.

#### 4.4. Alignment with conceptual hierarchy

When analyzing alignment with the conceptual hierarchy, we use the original ImageNet category labels for the images [Deng et al., 2009]. ImageNet is structured according to the WordNet hierarchy, from which we extract basic- and superordinate-categories that align with the prior cognitive work.

#### Acknowledgements

L.M., F.B., and K.R.M. were in part supported by the German Ministry for Education and Research (BMBF) under Grants 01IS14013A-E, 01GQ1115, 01GQ0850, 01IS18025A, 031L0207D, and 01IS18037A. K.R.M. was partly supported by the Institute of Information & Communications Technology Planning & Evaluation (IITP) grants funded by the Korean government (MSIT) (No. 2019-0-00079, Artificial Intelligence Graduate School Program, Korea University and No. 2022-0-00984, Development of Artificial Intelligence Technology for Personalized Plug-and-Play Explanation and Verification of Explanation). B.S. and F.B. were supported by European Research Council Consolidator Grant ERC-2020-COG-101000972 and Deutsche Forschungsgemeinschaft (DFG) Grant 462752742. Correspondence should be addressed to L.M., A.L., and K.R.M.

#### References

- I. M. Alabdulmohsin, X. Zhai, A. Kolesnikov, and L. Beyer. Getting ViT in shape: Scaling laws for compute-optimal model design. *Neural Information Processing Systems*, abs/2305.13035:16406–16425, 22 May 2023.
- G. Alain and Y. Bengio. Understanding intermediate layers using linear classifier probes. *International Conference on Learning Representations*, abs/1610.01644, 5 Oct. 2016.
- E. Amid and M. K. Warmuth. TriMap: Large-scale dimensionality reduction using triplets. *arXiv [cs.LG]*, 1 Oct. 2019.
- D. Amodei, C. Olah, J. Steinhardt, P. Christiano, J. Schulman, and D. Mané. Concrete problems in AI safety. *ArXiv*, abs/1606.06565, 21 June 2016.
- L. Beyer, O. J. H'enaff, A. Kolesnikov, X. Zhai, and A. van den Oord. Are we done with ImageNet? *ArXiv*, abs/2006.07159, 12 June 2020.
- L. Beyer, A. Steiner, A. S. Pinto, A. Kolesnikov, X. Wang, D. Salz, M. Neumann, I. Alabdulmohsin, M. Tschannen, E. Bugliarello, T. Unterthiner, D. Keysers, S. Koppula, F. Liu, A. Grycner, A. Gritsenko, N. Houlsby, M. Kumar, K. Rong, J. Eisenschlos, R. Kabra, M. Bauer, M. Bošnjak, X. Chen, M. Minderer, P. Voigtlaender, I. Bica, I. Balazevic, J. Puigcerver, P. Papalampidi, O. Henaff, X. Xiong, R. Soricut, J. Harmsen, and X. Zhai. PaliGemma: A versatile 3B VLM for transfer, 2024.
- D. Blei, A. Kucukelbir, and J. D. McAuliffe. Variational inference: A review for statisticians. *ArXiv*, 112:859–877, 4 Jan. 2016.
- C. Blundell, J. Cornebise, K. Kavukcuoglu, and D. Wierstra. Weight uncertainty in neural networks. *ArXiv*, abs/1505.05424, 20 May 2015.

J. Bowers, G. Malhotra, M. Dujmović, M. L. Montero, C. Tsvetkov, V. Biscione, G. Puebla, F. Adolfi, J. Hummel, R. Heaton, B. D. Evans, J. Mitchell, and R. Blything. Deep problems with neural network models of human vision. *The behavioral and brain sciences*, 46:1–74, 1 Dec. 2022.

M. B. Brodeur, K. Guérard, and M. Bouras. Bank of standardized stimuli (BOSS) phase II: 930 new normative photos. *PloS one*, 9(9):e106953, 11 Sept. 2014.

T. B. Brown, B. Mann, N. Ryder, M. Subbiah, J. Kaplan, P. Dhariwal, A. Neelakantan, P. Shyam, G. Sastry, A. Askell, S. Agarwal, A. Herbert-Voss, G. Krueger, T. Henighan, R. Child, A. Ramesh, D. M. Ziegler, J. Wu, C. Winter, C. Hesse, M. Chen, E. Sigler, M.-T. Litwin, S. Gray, B. Chess, J. Clark, C. Berner, S. McCandlish, A. Radford, I. Sutskever, and D. Amodei. Language models are few-shot learners. *Neural Information Processing Systems*, abs/2005.14165:1877–1901, 28 May 2020.

M. Caron, H. Touvron, I. Misra, H. Jegou, J. Mairal, P. Bojanowski, and A. Joulin. Emerging properties in self-supervised vision transformers. In *2021 IEEE/CVF International Conference on Computer Vision (ICCV)*. IEEE, Oct. 2021.

X. Chen, X. Wang, L. Beyer, A. Kolesnikov, J. Wu, P. Voigtlaender, B. Mustafa, S. Goodman, I. M. Alabdulmohsin, P. Padlewski, D. M. Salz, X. Xiong, D. Vlasic, F. Pavetic, K. Rong, T. Yu, D. Keysers, X.-Q. Zhai, and R. Soricut. PaLI-3 vision language models: Smaller, faster, stronger. *ArXiv*, abs/2310.09199, 13 Oct. 2023.

S. Chmiela, A. Tkatchenko, H. E. Sauceda, I. Poltavsky, K. T. Schütt, and K.-R. Müller. Machine learning of accurate energy-conserving molecular force fields. *Science advances*, 3(5):e1603015, 2017.

S. Chmiela, H. E. Sauceda, K.-R. Müller, and A. Tkatchenko. Towards exact molecular dynamics simulations with machine-learned force fields. *Nature communications*, 9(1):3887, 2018.

R. M. Cichy, N. Kriegeskorte, K. Jozwik, J. V. D. Bosch, and I. Charest. The spatiotemporal neural dynamics underlying perceived similarity for real-world objects. *NeuroImage*, 194:12–24, 1 July 2019.

A. C. Connolly, J. S. Guntupalli, J. D. Gors, M. Hanke, Y. Halchenko, Y.-C. Wu, H. Abdi, and J. Haxby. The representation of biological classes in the human brain. *The Journal of neuroscience: the official journal of the Society for Neuroscience*, 32(8):2608–2618, 22 Feb. 2012.

C. Conwell, J. S. Prince, K. N. Kay, G. A. Alvarez, and T. Konkle. What can 1.8 billion regressions tell us about the pressures shaping high-level visual representation in brains and machines? *bioRxiv*, 1 July 2023.

J. Deng, W. Dong, R. Socher, L.-J. Li, K. Li, and L. Fei-Fei. ImageNet: A large-scale hierarchical image database. In *2009 IEEE Conference on Computer Vision and Pattern Recognition*. IEEE, June 2009.

A. Dosovitskiy, L. Beyer, A. Kolesnikov, D. Weissenborn, X. Zhai, T. Unterthiner, M. Dehghani, M. Minderer, G. Heigold, S. Gelly, J. Uszkoreit, and N. Houlsby. An image is worth 16x16 words: Transformers for image recognition at scale. *International Conference on Learning Representations*, abs/2010.11929, 22 Oct. 2020.

A. Farahani, S. Voghoei, K. Rasheed, and H. R. Arabnia. A brief review of domain adaptation. In R. Stahlbock, G. M. Weiss, M. Abou-Nasr, C.-Y. Yang, H. R. Arabnia, and L. Deligiannidis, editors, *Advances in Data Science and Information Engineering*, pages 877–894, Cham, 2021. Springer International Publishing.

J. A. Fodor and Z. W. Pylyshyn. Connectionism and cognitive architecture: a critical analysis. *Cognition*, 28(1-2):3–71, Mar. 1988.

S. Fu, N. Y. Tamir, S. Sundaram, L. Chai, R. Zhang, T. Dekel, and P. Isola. DreamSim: Learning new dimensions of human visual similarity using synthetic data. *Neural Information Processing Systems*, abs/2306.09344:50742–50768, 15 June 2023.

K. Fukuzawa, M. Itoh, S. Sasanuma, T. Suzuki, Y. Fukusako, and T. Masui. Internal representations and the conceptual operation of color in pure alexia with color naming defects. *Brain and language*, 34(1):98–126, May 1988.

A. Geiger, A. Carstensen, M. C. Frank, and C. Potts. Relational reasoning and generalization using nonsymbolic neural networks. *Psychological review*, 130(2):308–333, Mar. 2023.

R. Geirhos, C. R. Medina Temme, J. Rauber, H. H. Schütt, M. Bethge, and F. Wichmann. Generalisation in humans and deep neural networks. *Neural Information Processing Systems*, 31:7549–7561, 27 Aug. 2018.

R. Geirhos, J.-H. Jacobsen, C. Michaelis, R. Zemel, W. Brendel, M. Bethge, and F. A. Wichmann. Shortcut learning in deep neural networks. *Nature machine intelligence*, 2(11):665–673, 10 Nov. 2020.

D. Gentner. Why we’re so smart. In D. Gentner and S. Goldin-Meadow, editors, *Language in Mind: Advances in the Study of Language and Thought*, pages 195–235. MIT Press, Cambridge, MA, 2003.

Y. Grandvalet and Y. Bengio. Semi-supervised learning by entropy minimization. *Conférence franco-phone sur l’apprentissage automatique*, 17:529–536, 1 Dec. 2004.

D. A. Grant. The latin square principle in the design and analysis of psychological experiments. *Psychological bulletin*, 45(5):427–442, 1 Sept. 1948.

A. Graves. Practical variational inference for neural networks. *Neural Information Processing Systems*, pages 2348–2356, 12 Dec. 2011.

C. Guo, G. Pleiss, Y. Sun, and K. Q. Weinberger. On calibration of modern neural networks. *International Conference on Machine Learning*, pages 1321–1330, 14 June 2017.

M. N. Hebart, A. H. Dickter, A. Kidder, W. Y. Kwok, A. Corriveau, C. Van Wicklin, and C. I. Baker. THINGS: A database of 1,854 object concepts and more than 26,000 naturalistic object images. *PloS one*, 14(10):e0223792, 15 Oct. 2019.

M. N. Hebart, C. Y. Zheng, F. Pereira, and C. I. Baker. Revealing the multidimensional mental representations of natural objects underlying human similarity judgements. *Nature human behaviour*, 4(11):1173–1185, Nov. 2020.

M. N. Hebart, O. Contier, L. Teichmann, A. H. Rockter, C. Y. Zheng, A. Kidder, A. Corriveau, M. Vaziri-Pashkam, and C. I. Baker. THINGS-data, a multimodal collection of large-scale datasets for investigating object representations in human brain and behavior. *eLife*, 12, 27 Feb. 2023.

D. Hendrycks and T. G. Dietterich. Benchmarking neural network robustness to common corruptions and perturbations. *International Conference on Learning Representations*, abs/1903.12261, 28 Mar. 2019.

D. Hendrycks, S. Basart, N. Mu, S. Kadavath, F. Wang, E. Dorundo, R. Desai, T. Zhu, S. Parajuli, M. Guo, D. Song, J. Steinhardt, and J. Gilmer. The many faces of robustness: A critical analysis of out-of-distribution generalization. In *Proceedings of the IEEE/CVF International Conference on Computer Vision*, pages 8340–8349, 2021a.

D. Hendrycks, K. Zhao, S. Basart, J. Steinhardt, and D. Song. Natural adversarial examples. *CVPR*, 2021b.

K. Hermann, H. Mobahi, T. Fel, and M. C. Mozer. On the foundations of shortcut learning. *International Conference on Learning Representations*, abs/2310.16228, 24 Oct. 2023.

K. L. Hermann, T. Chen, and S. Kornblith. The origins and prevalence of texture bias in convolutional neural networks. *Neural Information Processing Systems*, 20 Nov. 2019.

K. J. Holyoak and J. E. Hummel. The proper treatment of symbols in a connectionist architecture. In *Cognitive dynamics*, pages 229–263. Psychology Press, 2014.

C. Jia, Y. Yang, Y. Xia, Y.-T. Chen, Z. Parekh, H. Pham, Q. V. Le, Y.-H. Sung, Z. Li, and T. Duerig. Scaling up visual and vision-language representation learning with noisy text supervision. *International Conference on Machine Learning*, abs/2102.05918:4904–4916, 11 Feb. 2021.

G. E. Karniadakis, I. G. Kevrekidis, L. Lu, P. Perdikaris, S. Wang, and L. Yang. Physics-informed machine learning. *Nature Reviews Physics*, 3(6):422–440, 2021.

J. N. Kather, C.-A. Weis, F. Bianconi, S. Melchers, L. Schad, T. Gaiser, A. Marx, and F. Zöllner. Multi-class texture analysis in colorectal cancer histology. *Scientific reports*, 6, 16 June 2016.

R. Kiani, L. Corthell, and M. N. Shadlen. Choice certainty is informed by both evidence and decision time. *Neuron*, 84(6):1329–1342, 17 Dec. 2014.

M. L. King, I. I. A. Groen, A. Steel, D. J. Kravitz, and C. I. Baker. Similarity judgments and cortical visual responses reflect different properties of object and scene categories in naturalistic images. *NeuroImage*, 197:368–382, 15 Aug. 2019.

D. P. Kingma and M. Welling. Auto-Encoding Variational Bayes. *International Conference on Learning Representations*, abs/1312.6114, 20 Dec. 2013.

A. Kirillov, E. Mintun, N. Ravi, H. Mao, C. Rolland, L. Gustafson, T. Xiao, S. Whitehead, A. Berg, W.-Y. Lo, P. Dollár, and R. B. Girshick. Segment anything. *IEEE International Conference on Computer Vision*, pages 3992–4003, 5 Apr. 2023.

J. Krause, J. Deng, M. Stark, and L. Fei-Fei. Collecting a large-scale dataset of fine-grained cars, 2013.

N. Kriegeskorte, M. Mur, and P. Bandettini. Representational similarity analysis - connecting the branches of systems neuroscience. *Frontiers in systems neuroscience*, 2:4, 24 Nov. 2008a.

N. Kriegeskorte, M. Mur, D. A. Ruff, R. Kiani, J. Bodurka, H. Esteky, K. Tanaka, and P. A. Bandettini. Matching categorical object representations in inferior temporal cortex of man and monkey. *Neuron*, 60(6):1126–1141, Dec. 2008b.

A. Krizhevsky. Learning multiple layers of features from tiny images. Master’s thesis, University of Toronto, 2009.

B. M. Lake and M. Baroni. Human-like systematic generalization through a meta-learning neural network. *Nature*, 25 Oct. 2023.

B. M. Lake, R. Salakhutdinov, and J. B. Tenenbaum. Human-level concept learning through probabilistic program induction. *Science (New York, N.Y.)*, 350(6266):1332–1338, 11 Dec. 2015.

B. M. Lake, T. D. Ullman, J. B. Tenenbaum, and S. J. Gershman. Building machines that learn and think like people. *The behavioral and brain sciences*, 40(e253):e253, 2017.

S. Lapuschkin, A. Binder, G. Montavon, K.-R. Müller, and W. Samek. Analyzing classifiers: Fisher vectors and deep neural networks. In *2016 IEEE Conference on Computer Vision and Pattern Recognition (CVPR)*, pages 2912–2920. IEEE, June 2016.

S. Lapuschkin, S. Wäldchen, A. Binder, G. Montavon, W. Samek, and K.-R. Müller. Unmasking clever hans predictors and assessing what machines really learn. *Nature communications*, 10(1):1096, 11 Mar. 2019.

Y. LeCun, Y. Bengio, and G. Hinton. Deep learning. *Nature*, 521(7553):436–444, 28 May 2015.

D.-H. Lee. Pseudo-label : The simple and efficient semi-supervised learning method for deep neural networks. In *ICML 2013 workshop: Challenges in representation learning (WREPL)*, 2013.

G. F. Marcus. Rethinking eliminative connectionism. *Cognitive psychology*, 37(3):243–282, Dec. 1998.

J. L. McClelland, M. M. Botvinick, D. C. Noelle, D. C. Plaut, T. T. Rogers, M. S. Seidenberg, and L. B. Smith. Letting structure emerge: connectionist and dynamical systems approaches to cognition. *Trends in cognitive sciences*, 14(8):348–356, Aug. 2010.

M. Minderer, J. Djolonga, R. Romijnders, F. Hubis, X. Zhai, N. Houlsby, D. Tran, and M. Lucic. Revisiting the calibration of modern neural networks. *Neural Information Processing Systems*, abs/2106.07998: 15682–15694, 15 June 2021.

L. Muttenthaler, C. Zheng, P. McClure, R. A. Vandermeulen, M. Hebart, and F. Pereira. VICE: Variational Interpretable Concept Embeddings. *Neural Information Processing Systems*, abs/2205.00756, 2 May 2022.

L. Muttenthaler, J. Dippel, L. Linhardt, R. A. Vandermeulen, and S. Kornblith. Human alignment of neural network representations. *International Conference on Learning Representations*, abs/2211.01201, 3 Apr. 2023a.

L. Muttenthaler, L. Linhardt, J. Dippel, R. A. Vandermeulen, K. L. Hermann, A. K. Lampinen, and S. Kornblith. Improving neural network representations using human similarity judgments. *Neural Information Processing Systems*, abs/2306.04507, 7 June 2023b.

L. Muttenthaler, R. A. Vandermeulen, Q. Zhang, T. Unterthiner, and K.-R. Müller. Set learning for accurate and calibrated models. *International Conference on Learning Representations*, abs/2307.02245, 5 July 2024.

M.-E. Nilsback and A. Zisserman. Automated flower classification over a large number of classes. In *2008 Sixth Indian Conference on Computer Vision, Graphics & Image Processing*, pages 722–729. IEEE, Dec. 2008.

OpenAI, J. Achiam, S. Adler, S. Agarwal, L. Ahmad, I. Akkaya, F. L. Aleman, D. Almeida, J. Altenschmidt, S. Altman, S. Anadkat, R. Avila, I. Babuschkin, S. Balaji, V. Balcom, P. Baltescu, H. Bao, M. Bavarian, J. Belgum, I. Bello, J. Berdine, G. Bernadett-Shapiro, C. Berner, L. Bogdonoff, O. Boiko, M. Boyd, A.-L. Brakman, G. Brockman, et al. GPT-4 technical report. *arXiv [cs.CL]*, 15 Mar. 2023.

M. Oquab, T. Darcet, T. Moutakanni, H. Q. Vo, M. Szafraniec, V. Khalidov, P. Fernandez, D. Haziza, F. Massa, A. El-Nouby, M. Assran, N. Ballas, W. Galuba, R. Howes, P.-Y. b. Huang, S.-W. Li, I. Misra, M. G. Rabbat, V. Sharma, G. Synnaeve, H. Xu, H. Jégou, J. Mairal, P. Labatut, A. Joulin, and P. Bojanowski. DINOv2: Learning robust visual features without supervision. *ArXiv*, abs/2304.07193, 14 Apr. 2023.

A. Paleyes, R.-G. Urma, and N. D. Lawrence. Challenges in deploying machine learning: A survey of case studies. *ACM computing surveys*, 55(6):1–29, 31 July 2023.

O. M. Parkhi, A. Vedaldi, A. Zisserman, and C. V. Jawahar. Cats and dogs. In *2012 IEEE Conference on Computer Vision and Pattern Recognition*, pages 3498–3505. IEEE, June 2012.

D. C. Penn, K. J. Holyoak, and D. J. Povinelli. Darwin’s mistake: Explaining the discontinuity between human and nonhuman minds. *The behavioral and brain sciences*, 31(2):109–130, Apr. 2008.

J. Peterson, R. Battleday, T. Griffiths, and O. Russakovsky. Human uncertainty makes classification more robust. In *2019 IEEE/CVF International Conference on Computer Vision (ICCV)*. IEEE, Oct. 2019.

J. C. Peterson, J. T. Abbott, and T. Griffiths. Adapting deep network features to capture psychological representations. *Annual Meeting of the Cognitive Science Society*, abs/1608.02164, 1 Aug. 2016.

J. C. Peterson, J. T. Abbott, and T. L. Griffiths. Evaluating (and improving) the correspondence between deep neural networks and human representations. *Cognitive science*, 42(8):2648–2669, Nov. 2018.

E. Pooch, P. Ballester, and R. C. Barros. Can we trust deep learning models diagnosis? the impact of domain shift in chest radiograph classification. *ArXiv*, abs/1909.01940:74–83, 3 Sept. 2019.

V. Puatruauean, L. Smaira, A. Gupta, A. R. Continente, L. Markeeva, D. Banarse, S. Koppula, J. Heyward, M. Malinowski, Y. Yang, C. Doersch, T. Matejovicova, Y. Sulsky, A. Miech, A. Fréchette, H. Klimczak, R. Koster, J. Zhang, S. Winkler, Y. Aytar, S. Osindero, D. Damen, A. Zisserman, and J. a. Carreira. Perception test: A diagnostic benchmark for multimodal video models. *Neural Information Processing Systems*, abs/2305.13786, 23 May 2023.

A. Radford, J. W. Kim, C. Hallacy, A. Ramesh, G. Goh, S. Agarwal, G. Sastry, A. Askell, P. Mishkin, J. Clark, G. Krueger, and I. Sutskever. Learning transferable visual models from natural language supervision. *International Conference on Machine Learning*, pages 8748–8763, 26 Feb. 2021.

R. Ratcliff. A theory of memory retrieval. *Psychological review*, 85(2):59–108, 1978.

B. Recht, R. Roelofs, L. Schmidt, and V. Shankar. Do ImageNet classifiers generalize to ImageNet? *International Conference on Machine Learning*, 97:5389–5400, 13 Feb. 2019.

D. J. Rezende, S. Mohamed, and D. Wierstra. Stochastic backpropagation and approximate inference in deep generative models. *International Conference on Machine Learning*, pages 1278–1286, 16 Jan. 2014.

B. D. Roads and M. C. Mozer. Improving human-machine cooperative classification via cognitive theories of similarity. *Cognitive science*, 41(5):1394–1411, July 2017.

R. Robilotto and Q. Zaidi. Limits of lightness identification for real objects under natural viewing conditions. *Journal of vision*, 4(9):779–797, 15 Sept. 2004.

E. Rosch, C. B. Mervis, W. D. Gray, D. M. Johnson, and P. Boyes-Braem. Basic objects in natural categories. *Cognitive psychology*, 8(3):382–439, July 1976.

O. Russakovsky, J. Deng, H. Su, J. Krause, S. Satheesh, S. Ma, Z. Huang, A. Karpathy, A. Khosla, M. S. Bernstein, A. Berg, and L. Fei-Fei. ImageNet large scale visual recognition challenge. *International journal of computer vision*, 115:211–252, 1 Sept. 2014.

S. Santurkar, D. Tsipras, and A. Madry. BREEDS: Benchmarks for subpopulation shift. *International Conference on Learning Representations*, abs/2008.04859, 11 Aug. 2020.

N. F. Schmitz, K.-R. Müller, and S. Chmiela. Algorithmic differentiation for automated modeling of machine learned force fields. *The Journal of Physical Chemistry Letters*, 13(43):10183–10189, 2022.

I. Sucholutsky, L. Muttenthaler, A. Weller, A. Peng, A. Bobu, B. Kim, B. C. Love, E. Grant, J. Achterberg, J. B. Tenenbaum, K. M. Collins, K. L. Hermann, K. Oktar, K. Greff, M. Hebart, N. Jacoby, Q. Zhang, R. Marjieh, R. Geirhos, S. Chen, S. Kornblith, S. Rane, T. Konkle, T. P. O’Connell, T. Unterthiner, A. K. Lampinen, K.-R. Müller, M. Toneva, and T. L. Griffiths. Getting aligned on representational alignment. *ArXiv*, abs/2310.13018, 18 Oct. 2023.

M. Sugiyama and M. Kawanabe. *Machine learning in non-stationary environments: Introduction to covariate shift adaptation*. Adaptive Computation and Machine Learning. Mit Press, London, England, 1 Jan. 2012.

M. Sugiyama, M. Krauledat, and K.-R. Müller. Covariate shift adaptation by importance weighted cross validation. *Journal of machine learning research: JMLR*, 8(5):985–1005, 1 Dec. 2007.

G. Team, R. Anil, S. Borgeaud, Y. Wu, J.-B. Alayrac, J. Yu, R. Soricut, J. Schalkwyk, A. M. Dai, and A. Hauth. Gemini: a family of highly capable multimodal models. *arXiv preprint arXiv:2312.11805*, 2023.

J. B. Tenenbaum, C. Kemp, T. L. Griffiths, and N. D. Goodman. How to grow a mind: statistics, structure, and abstraction. *Science (New York, N.Y.)*, 331(6022):1279–1285, 11 Mar. 2011.

T. Thrush, R. Jiang, M. Bartolo, A. Singh, A. Williams, D. Kiela, and C. Ross. Winoground: Probing vision and language models for visio-linguistic compositionality. In *2022 IEEE/CVF Conference on Computer Vision and Pattern Recognition (CVPR)*, pages 5238–5248. IEEE, June 2022.

M. Tschannen, M. Kumar, A. Steiner, X. Zhai, N. Houlsby, and L. Beyer. Image captioners are scalable vision learners too. *Neural Information Processing Systems*, abs/2306.07915, 13 June 2023.

J. Waltz, B. Knowlton, K. Holyoak, K. Boone, F. Mishkin, M. de Menezes Santos, C. Thomas, and B. Miller. A system for relational reasoning in human prefrontal cortex. *Psychological science*, 10(2):119–125, 1 Mar. 1999.

Y. Wang, Q. Yao, J. T. Kwok, and L. M. Ni. Generalizing from a few examples: A survey on few-shot learning. *ACM computing surveys*, 53(3):1–34, 31 May 2021.

P. Welinder, S. Branson, T. Mita, C. Wah, F. Schroff, S. J. Belongie, and P. Perona. Caltech-UCSD birds 200, 29 Sept. 2010.

Y. Yang and S. Newsam. Bag-of-visual-words and spatial extensions for land-use classification. In *Proceedings of the 18th SIGSPATIAL International Conference on Advances in Geographic Information Systems*, New York, NY, USA, 2 Nov. 2010. ACM.

X. Zhai, B. Mustafa, A. Kolesnikov, and L. Beyer. Sigmoid loss for language image pre-training. *IEEE International Conference on Computer Vision*, pages 11941–11952, 27 Mar. 2023.

B. Zhou, A. Lapedriza, A. Khosla, A. Oliva, and A. Torralba. Places: A 10 million image database for scene recognition. *IEEE transactions on pattern analysis and machine intelligence*, 40(6):1452–1464, 1 June 2018.

## Supplement

### A. Methods

#### A.1. AligNet framework

This section is organized as follows: We start by describing how we transform model representations into a space that matches human similarity judgments about coarse-grained semantic object relations. We introduce a novel affine transformation that matches human similarity judgments and injects the uncertainties that humans assign to their triplet odd-one-out choices into a model’s representation space. Using these human-aligned representations, we sample triplets of ImageNet [Deng et al., 2009] images differently than uniform random sampling by clustering the representations into superordinate categories and using those clusters for data partitioning. Finally, after having created AligNet triplets, we can fine-tune models with a novel triplet loss object function.

##### A.1.1. *Representational alignment*

**Data.** To increase the degree of alignment between human and neural network similarity spaces, we use the publicly available THINGS dataset, which is a large behavioral dataset of 4.7 million unique triplet responses from 12,340 human participants for  $m = 1854$  natural object images [Hebart et al., 2023] from the public THINGS object concept and image database [Hebart et al., 2019]. Let  $\mathcal{D}_{\text{things}} := (\{a_s, b_s\} \mid \{i_s, j_s, k_s\})_{s=1}^n$  be the dataset of object triplets and corresponding human responses, where  $\{a, b\} \subset \{i, j, k\}$  and  $\{a, b\}$  is the object pair that was chosen by a human participant to have the highest similarity.

**Odd-one-out accuracy.** The triplet odd-one-out task is a commonly used task in the cognitive sciences to measure human notions of object similarity [Fukuzawa et al., 1988; Robilotto and Zaidi, 2004; Hebart et al., 2020; Muttenthaler et al., 2022]. To measure the degree of alignment between human and neural network similarity judgments in the THINGS triplet task, we embed the  $m = 1854$  THINGS images into the representation space of a neural network with  $X \in \mathbb{R}^{m \times p}$ . Given vector representations  $x_1, x_2$ , and  $x_3$  of the three images in a triplet, we first construct a similarity matrix  $S \in \mathbb{R}^{3 \times 3}$  where  $S_{i,j} := x_i^\top x_j$  is the dot product between a pair of image representations. We identify the closest pair of images in the triplet as  $\arg \max_{i,j>i} S_{i,j}$  with the remaining image being the odd-one-out. We define odd-one-out accuracy as the fraction of triplets where the odd-one-out “chosen by a model” is identical to the human odd-one-out choice. Thus, we want to find an affine transformation of the general form  $x' = Wx + b$  with  $x' \in \mathbb{R}^p$  that maximizes this accuracy. The pairwise similarity can then be defined as  $S'_{ij} = (Wx_i + b)^\top (Wx_j + b)$ .

**Hard alignment loss.** Given a similarity matrix of neural network representations  $S$  and a triplet  $\{i, j, k\}$ , the likelihood of a particular pair,  $\{a, b\} \subset \{i, j, k\}$ , being most similar with the remaining object being the odd-one-out, is modeled by the softmax of the object similarities,

$$\sigma(S, \tau) := \exp(S_{a,b}/\tau) / (\exp(S_{i,j}/\tau) + \exp(S_{i,k}/\tau) + \exp(S_{j,k}/\tau)). \quad (4)$$

We can then define the probability of the neural network model to choose the most similar pair (according to the human subjects) to be  $q(\{a, b\} \mid \{i, j, k\}, S) := \sigma(S, \tau)$  with  $\tau = 1$ . For  $n$  triplet responses, the discrete negative log-likelihood is defined as follows,

$$\mathcal{L}_{\text{hard-align}}(S') := -\frac{1}{n} \sum_{s=1}^n \log \underbrace{q(\{a_s, b_s\} \mid \{i_s, j_s, k_s\}, S')}_{\text{odd-one-out prediction}}.$$

**Modelling human uncertainties.** Since each triplet response is a discrete choice, we don’t have direct access to the uncertainties of a human participant over the objects in a triplet. Thus, the

above loss function optimizes a transform to match the human choice but does not take into account the uncertainties over the three odd-one-out alternatives. However, it is possible to model these uncertainties using Variational Interpretable Concept Embeddings [VICE; [Muttenthaler et al., 2022](#)], a recently proposed, approximate Bayesian inference method for learning an interpretable object concept space from human similarity judgments. VICE has shown remarkable performance in predicting the (dis-)agreement in human similarity judgments for multiple similarity judgment datasets, including THINGS [[Muttenthaler et al., 2022](#)].

We train a VICE model on the official THINGS train triplet dataset using the (default) hyperparameters recommended by the authors. To capture the uncertainties in human triplet responses, VICE learns a mean,  $\mu \in \mathbb{R}^{m \times d}$ , and a variance,  $\sigma \in \mathbb{R}^{m \times d}$ , for each object image and each object dimension respectively. Therefore, the set of VICE parameters is defined as  $\theta = \{\mu, \sigma\}$ . VICE uses the reparameterization trick [[Kingma and Welling, 2013](#); [Rezende et al., 2014](#)] to generate an embedding matrix  $Y \in \mathbb{R}^{m \times d}$ ,  $Y_{\theta, \epsilon} = \mu + \sigma \odot \epsilon$ , where  $\epsilon \in \mathbb{R}^{m \times d}$  is entrywise  $\mathcal{N}(0, 1)$ , and  $\odot$  denotes the Hadamard (element-wise) product.

After convergence, we can use a VICE model to obtain a posterior probability distribution for each triplet in the data. We approximate the probability distribution using a Monte Carlo estimate [[Graves, 2011](#); [Blundell et al., 2015](#); [Blei et al., 2016](#)] from  $R$  samples  $Y^{(r)} = Y_{\hat{\theta}, \epsilon^{(r)}}$  for  $r = 1, \dots, R$ , yielding

$$\hat{p}(\{y_s, z_s\} | \{i_s, j_s, k_s\}) := \frac{1}{R} \sum_{r=1}^R \underbrace{p(\{y_s, z_s\} | \{i_s, j_s, k_s\}, Y^{(r)})}_{\text{Monte-Carlo estimate(s)}},$$

where we set  $R = 50$  because we found it to yield the best predictive performance on the official THINGS validation set. This gives a representative probability estimate for each of the three pairs in a triplet to be selected as the most similar pair.

**Soft alignment loss.** Using the posterior probability estimates obtained from VICE, we transform the original THINGS triplet dataset of discrete triplet choices into a triplet dataset of probability distributions that reflect the human uncertainties of the triplet alternatives. Let  $\mathcal{D}^\dagger := (p_s^*(\{i_s, j_s, k_s\}))_{s=1}^n$  be the transformed triplet dataset, where

$$p_s^*(\{i_s, j_s, k_s\}) := \hat{p}(\{y_s, z_s\} | \{i_s, j_s, k_s\}) \quad \forall \{y, z\} \subset \{i, j, k\}.$$

Now, for  $n$  triplet responses we can define the negative log-likelihood for the soft alignment loss as,

$$\mathcal{L}_{\text{soft-align}}(\mathbf{S}') := \frac{1}{n} \sum_{s=1}^n \underbrace{\log p_s^*(\{i_s, j_s, k_s\})}_{\text{human uncertainty}} - \underbrace{p_s^*(\{i_s, j_s, k_s\}) \log q_s(\{i_s, j_s, k_s\}, \mathbf{S}')}_{\text{cross-entropy}},$$

where  $q_s(\{i_s, j_s, k_s\}, \mathbf{S}) := q(\{y_s, z_s\} | \{i_s, j_s, k_s\}, \mathbf{S}) \quad \forall \{y, z\} \subset \{i, j, k\}$ .

**Uncertainty distillation.** Using the above soft alignment loss function instead of the vanilla hard alignment loss proposed by [Muttenthaler et al. \[2023a\]](#) for aligning the model representations with human global object similarity, the final objective function for the *uncertainty distillation (UD)* transformation is defined as follows,

$$\arg \min_{W, b} \underbrace{\mathcal{L}_{\text{soft-align}}(X, W, b)}_{\text{soft alignment}} + \lambda \left\| W - \left( \sum_{j=1}^p W_{jj} / p \right) I \right\|_F^2.$$

Although this expression is similar to the global transform defined in [Muttenthaler et al. \[2023b\]](#), we find it to yield equally strong downstream task performance as the gLocal transform proposed in

[Muttenthaler et al. \[2023b\]](#) while predicting human uncertainties better than the global transform. It appears as if there is barely any trade-off between representational alignment and downstream task performance for using the UD, whereas [Muttenthaler et al. \[2023b\]](#) found that the global transform yields slightly better human alignment but worse downstream task performance compared to the gLocal transform. We use the UD transformation for generating human-like similarity judgments by transforming a model’s representation space with UD.

### A.1.2. Data generation

In the following section, we describe the AligNet data generation process. We start by introducing the data that we use for constructing the triplets. We continue with a detailed description of the different sampling strategies that we consider in our analyses. Finally, we explain how we collect model responses using transformed representations and define the objective function for fine-tuning models on AligNet.

**Image data.** For creating AligNet, we use the publicly available ImageNet database [[Deng et al., 2009](#)]. ImageNet is a natural image dataset with  $\approx 10^6$  training data points and 1000 image categories [[Russakovsky et al., 2014](#)]. The categories are almost equally distributed in the data with small variations in the number of images between the different classes. Hence, ImageNet can be considered a highly balanced dataset. ImageNet has been the dominant image dataset for training large computer vision models until the advent of image/text multi-modal training a few years ago. Although to date larger image datasets exist, ImageNet is still one of the largest open-source and most widely used image datasets in the field of Computer Vision.

**Triplet sampling.** For generating triplets of images, we employ three different sampling strategies: *random*, *class-border*, and *cluster-boundary* sampling. Let  $m'$  be the number of images in the data where  $m' = 1,281,167$  and  $C$  be the number of classes with  $C = 1000$ . Let  $\mathcal{D}_{\text{image}} := (x_i, y_i)_{i=1}^{m'}$  be the ImageNet dataset of  $m'$  image-label pairs.

**Random.** Uniform random sampling is the vanilla sampling approach and was used to create the THINGS datasets (see Sec. A.1.1). In random sampling, three images are chosen uniformly at random without replacement from all of the  $m$  images in the data to create a triplet. Since there are  $C = 1000$  classes and each class has approximately 1000 images, most of the triplets generated with this approach contain three images from three different classes. The number of triplets different from triplets with images from three distinct classes is negligible. Note that this is the same sampling approach that was used to generate the THINGS triplets [[Hebart et al., 2020](#)]. A triplet generated via random sampling can be defined as the following triplet set  $S := \{x_i, x_j, x_k\}$  with the constraint  $(y_i \neq y_j \neq y_k)$ .

**Class-boundary.** Another way to sample image triplets is to exploit the label information associated with each data point. Instead of three random images from three distinct classes, we determine class-boundary triplets to contain two images from the same class and one image from a different class. This is similar to the approach introduced in [Muttenthaler et al. \[2024\]](#) where each odd- $k$ -out set of images contains a majority class and  $k$  odd class singletons. This sampling approach allows models to learn class boundaries similar to the standard supervised learning setting. A triplet generated via class-boundary sampling can be defined as the following triplet set  $S := \{x_i, x_j, x_k\}$  with the constraint  $(y_i = y_j \neq y_k) \vee (y_i \neq y_j = y_k) \vee (y_i = y_k \neq y_j)$  where the original labels are used for data partitioning.

**Cluster-boundary.** Since we want to introduce a general approach that does not rely on label information, we employ a third sampling strategy that is in principle similar to the class-boundary approach but does not require labels. Let  $Z \in \mathbb{R}^{m' \times p}$  be the stacked representations of a neural network model for every image in  $\mathcal{D}_{\text{image}}$ . The representations can essentially be computed for any layer of a

model. Here, we use the image encoder for image/text models and the `cls` token representation of the penultimate layer for any other model (since we only use ViT based models).

We cluster the representation spaces  $Z$  and  $Z' := (WZ^\top + [b_1, \dots, b_{m'}])^\top$ <sup>1</sup> respectively (see Sec. 3 for how the transformation variables  $W$  and  $b$  are computed) into  $c$  representation clusters where  $c$  can be regarded as similar to  $C$ , the number of labels in the original dataset. We use the Elbow criterion to select  $c$ . For all of our main experiments we set  $c = 500$ . Hence, the ImageNet dataset is transformed into a dataset of image-cluster instead of image-label pairs. Let  $\mathcal{D}'_{\text{image}} := (x_i, y'_i)_{i=1}^{m'}$  be the modified ImageNet dataset of image and cluster pairs. After the clustering, we apply the same sampling method as for class-boundary triplets: for each triplet we choose uniformly at random two images without replacement from one cluster and one image from a different cluster. Thus, a triplet generated via cluster-boundary sampling can be defined as the following set  $\mathcal{S} := \{x_i, x_j, x_k\}$  with the constraint  $(y'_i = y'_j \neq y'_k) \vee (y'_i \neq y'_j = y'_k) \vee (y'_i = y'_k \neq y'_j)$  where instead of the original labels we use the cluster labels for partitioning the data.

**Triplet response generation** Let  $\mathcal{D}_{\text{triplets}} := (\{x_i, x_j, x_k\}_s)_{s=1}^{n'}$  be the dataset of sampled ImageNet triplets for which we want to collect responses using transformed model representations. Note that we can sample an arbitrary number of triplets — upper-bounded by the binomial coefficient  $\binom{n'}{k}$  with  $k = 3$  — and can thus set  $n'$  to essentially any natural number. For the experiments that we report in the main text we set  $n' = 10^7$  because we found a larger  $n'$  to not yield any downstream task improvements. For now, we regard our surrogate model as a blackbox model with transformed ImageNet representations  $Z' := (WZ^\top + [b_1, \dots, b_{m'}])^\top \in \mathbb{R}^{m' \times p}$  where the affine transformation was found via UD optimization (see Eq. 3).

Given transformed representations  $z'_1, z'_2$ , and  $z'_3$  of the three images in a triplet, we can construct a similarity matrix  $S' \in \mathbb{R}^{3 \times 3}$  where  $S'_{i,j} := z'_i^\top z'_j$  is the dot product between a pair of representations. Similarly to how we do this for learning the UD transformation (see Sec. A.1.1), we identify the closest pair of images in a triplet as  $\arg \max_{i,j>i} S'_{i,j}$  with the remaining image being the odd-one-out. Let  $\mathcal{D}_{\text{align}} := (\{x_a, x_b\}_s \mid \{x_i, x_j, x_k\}_s)_{s=1}^{n'}$  then constitute the final AligNet dataset of ImageNet triplets and corresponding model responses, where  $\{x_a, x_b\} \subset \{x_i, x_j, x_k\}$  and  $\{x_a, x_b\}$  is the image pair that was chosen by the transformed model representations to have the highest pairwise similarity. The model choices are the closest approximation to the human choices due to the UD transformation.

### A.1.3. Objective function

Let  $f_\theta$  be a neural network function parameterized by  $\theta$ , the set of its weights and biases. For every input image  $x$  that the function  $f_\theta(x)$  processes it yields a representation  $f_\theta(x) = z$ . Here,  $z$  refers to the image encoder representation of image/text models or the `cls` token representation before the final linear layer for other model types. From the representations of the three images in a triplet, we can again construct a similarity matrix  $S^\dagger \in \mathbb{R}^{3 \times 3}$  where  $S^\dagger_{i,j} := z_i^\top z_j$  is the dot product between a pair of image representations. The AligNet loss function is defined as the following KL divergence between teacher and student triplet probabilities,

$$\mathcal{L}_{\text{alignnet}}(S', S^\dagger) := \frac{1}{B} \sum_{s=1}^B \log \sigma \left( \left[ S'_{i,j}, S'_{i,j}, S'_{j,k} \right], \tau' \right)_s - \sigma \left( \left[ S'_{i,j}, S'_{i,j}, S'_{j,k} \right], \tau' \right)_s \log \sigma \left( \left[ S^\dagger_{i,j}, S^\dagger_{i,k}, S^\dagger_{j,k} \right], \tau^\dagger \right)_s, \quad (5)$$

where  $\tau' = 1$  and  $\tau^\dagger > 1$  and  $B$  is the batch size. We find  $\tau^\dagger$  via grid search and set it to  $\tau^\dagger = 100$  for all of our experiments. Recall that  $\sigma$  is a softmax function that models the probabilities over the three

<sup>1</sup>Each of the  $m$  column vectors on the right-hand side is the same  $b$ .

image similarity pairs (see Eq. 4). The final AligNet objective is defined as the following minimization problem,

$$\arg \min_{\theta} \mathcal{L}_{\text{alignet}}(f_{\theta}) + \lambda \|\theta^* - \theta^{\dagger}\|_2^2, \quad (6)$$

where  $\theta^*$  are the parameters of the pretrained base student model and  $\theta^{\dagger}$  are the parameters of the fine-tuned student model. This  $\ell_2$ -regularization, which we refer to as *weight decay to initialization*, encourages the fine-tuned set of parameters to stay close to its base during training. It is similar to the regularization employed for learning the UD transformation (see Eq. 3) but adapted to the set of all model parameters rather than a linear transform.

#### A.1.4. Surrogate teacher model

[Muttenhaller et al. \[2023a\]](#) showed that image/text models and models trained on large, diverse datasets are better aligned with human similarity judgments than vision models trained with a self-supervised learning objective or supervised models trained on ImageNet. Thus, we use the best-performing image/text model according to various computer vision benchmarks at the time of writing this manuscript as our teacher model. This model is called SigLIP [[Zhai et al., 2023](#)]. SigLIP, similar to CLIP [[Radford et al., 2021](#)] and ALIGN [[Jia et al., 2021](#)], is trained via contrastive language-image pretraining using millions of image/text pairs. The difference between CLIP and SigLIP is that SigLIP uses a paired sigmoid loss instead of the standard softmax function usually used for pretraining image/text models via cross-entropy. Image/text pretraining allows the model to learn an aligned representation space for images and text; thus, adding more semantic information about the objects in an image to the model representations.

We use the SigLIP-So400m variant of SigLIP as our teacher model. The So400m variant uses an optimized ViT backbone whose performance is similar to one of the largest ViTs, ViT-g/14 [[Alabdulmohsin et al., 2023](#)] while having fewer parameters and thus being smaller. The number of parameters of SoViT-400m/14 lies somewhere between ViT-L/16 and ViT-g/14. The output dimensionality of the image and text encoder representations of SoViT-400m/14 is  $p=1152$  each. We align the image encoder representations with human odd-one-out choices using the UD optimization outlined in Eq. 6. This allows us to increase the triplet odd-one-out accuracy of SigLIP-So400m from 44.24% to 61.7% (see rightmost column in Tab. 1) which is close to the human-noise ceiling of 66.67% for THINGS [c.f. [Hebart et al., 2020](#)] and thus among the best human-aligned models without AligNet fine-tuning [c.f. [Muttenhaller et al., 2023a](#)]. Note that this is a relative increase in performance of 39.47%. Throughout this manuscript we use the human-aligned version of SigLIP-So400m as the *surrogate teacher model* for generating human-like similarity judgments and distilling human-like similarity structure into student VFM. We select a diverse and representative set of student VFM.

#### A.1.5. Student Models

Since previous research has demonstrated that a model’s architecture has no significant impact on the degree of alignment with human similarity judgments [[Muttenhaller et al., 2023a,b](#)], we use the same architecture for all student models that we fine-tune on AligNet. Specifically, we use the Vision Transformer [ViT; [Dosovitskiy et al., 2020](#)] for the backbone of each student model. We use the ViT rather than CNN-based model because ViTs have recently emerged as the dominant neural network architecture for computer vision application and VFM. Every large VFM that is used in practice is based on the ViT [[Tschannen et al., 2023](#); [Chen et al., 2023](#); [Zhai et al., 2023](#); [Beyer et al., 2024](#)]. Unless otherwise mentioned, we use the base model size, i.e., ViT-B. ViT-B has 12 attention layers and an internal (hidden) representation size of  $p = 768$ . It has been shown that both the training data and the objective function have a substantial impact on the degree of alignment with human

behavior. Thus, we use student models that were trained on different pretraining task with different training data and objective functions.

*Supervised* pre-training is still the prevailing mode of training computer vision models. Therefore, we trained ViT-B on the popular ImageNet dataset consisting of 1.4M natural images [Deng et al., 2009]. To examine how model performance changes as a function of the size of a model, we train ViT instances of three different sizes on ImageNet: ViT-S/16, ViT-B/16, ViT-L/16. The image patch size is the same for each of those models. To evaluate the effect of AligNet on *self-supervised* pretraining, we use pretrained DINOv1 [Caron et al., 2021] and DINOv2 [Oquab et al., 2023] models of which DINOv1 was pretrained on ImageNet and DINOv2 was pretrained on a different, larger image dataset as denoted below. In addition, we investigate *multimodal training of vision models* that add textual information both in the form of *image captioning* via the CapPa model [Tschanne et al., 2023], as well as *contrastive language-image pretraining* (CLIP) via SigLIP [Zhai et al., 2023]. The latter model is considered *state-of-the-art* on many downstream computer vision applications and is used as the image embedding model in modern large visual-language models [VLMs; Chen et al., 2023; Beyer et al., 2024]. The full list of student models that we consider in our analyses is the following:

- ViT-{S,B,L}
  - *Training data*: ImageNet [Deng et al., 2009]
  - *Objective*: Supervised learning
- SigLIP-{B,SO400M}
  - *Training data*: WebLI [Zhai et al., 2023]
  - *Objective*: CLIP [Radford et al., 2021]
- DINOv1 (ViT-B)
  - *Training data*: ImageNet [Deng et al., 2009]
  - *Objective*: Self-supervised image pretraining [Caron et al., 2021]
- DINOv2 (ViT-B)
  - *Training data*: DINOv2 data (see Oquab et al. [2023] for details)
  - *Objective*: Self-supervised teacher-student distillation [Oquab et al., 2023]
- CapPa (ViT-B)
  - *Training data*: JFT-3B (Google proprietary dataset)
  - *Objective*: Multi-modal image captioning [Tschanne et al., 2023]

## A.2. Representational Similarity Analysis (RSA)

### A.2.1. Multi-arrangement task

Human similarity judgments for King et al. [2019] and Cichy et al. [2019] were obtained by using a multi-arrangement task. In a multi-arrangement task, participants are presented with a computer screen showing images of several different objects. The participants are asked to arrange the images into semantically meaningful clusters, given the instruction that images of objects that lie close together are considered more similar. From this arrangement, one can infer pairwise (dis-)similarities of the objects and average those across all participants to obtain a representative (dis-)similarity matrix.

### A.2.2. Likert scale

In Peterson et al. [2016, 2018], pairwise similarity judgments were obtained by asking human participants to rate the similarity of pairs of objects on an ordinal scale that ranges from 0 (“not

similar at all”) to 10 (“very similar”). The pairwise similarity ratings can be averaged across the different participants which in turn yields a matrix of similarities between pairs of objects.

### A.2.3. Neural network representations

Representation Similarity Matrices (RSMs) for neural network representations are obtained by first embedding the same set of images that were presented to the human participants in the  $p$ -dimensional latent space of a model. The latent space could be any layer of a neural network. For the base models, we use the representations of the image encoder for SigLIP and the CLS token of the penultimate layer for CapPa, DINOv2, and ViT-B. We do this because previous work has shown that the penultimate layer space and the image encoder space of image/text models respectively yield the highest similarity to human behavior [Peterson et al., 2018, 2019; Muttenthaler et al., 2023a].

After embedding the images into the neural net’s latent space, we get a representation matrix  $X \in \mathbb{R}^{n \times p}$  for the  $n$  images in the data. Instead of simply computing the dot-product similarity matrix  $S := XX^\top$ , in RSA one typically uses either a cosine similarity or a Pearson correlation kernel to compute the affinity matrix,

$$\cos(x_i, x_j) := \frac{x_i^\top x_j}{\|x_i\|_2 \|x_j\|_2}; \quad \phi(x_i, x_j) := \frac{(x_i - \bar{x}_i)^\top (x_j - \bar{x}_j)}{\| (x_i - \bar{x}_i) \|_2 \| (x_j - \bar{x}_j) \|_2},$$

where the cosine similarity kernel function  $\cos(x_i, x_j)$  or the Pearson correlation kernel function  $\phi(x_i, x_j)$  is applied to every  $(x_i, x_j)$  vector pair of the matrix  $X$  for obtaining the final representational similarity matrix  $S' \in \mathbb{R}^{n \times n}$ . Here, we use the Pearson correlation kernel function  $\phi(x_i, x_j)$  to obtain a neural net’s RSM. Pearson correlation is the centered version of cosine similarity and the ranking of the obtained similarities does not differ between the two kernel functions but Pearson correlation first centers the vectors to have zero mean and is therefore a more robust measure. For obtaining RSMs with transformed representations, the transforms are first applied to  $X$  before computing  $S'$ .

## A.3. Levels data

**Participants.** We recruited  $N = 508$  participants (209 female, 289 male, 3 diverse,  $N = 7$  missing demographic information due to revocation of study consent; mean age =  $31.75 \pm \text{SD: } 8.04$  years) online via Prolific Academic (<https://www.prolific.ac>). The eligibility criteria were that participants had to be between 18 and 50 years old, fluent in English, have a normal or corrected-to-normal vision, no colorblindness, and have a minimum approval rating of 95% on Prolific. Participants provided informed consent before starting the experiment. The experiment lasted approximately 45 minutes. Participants were reimbursed with £7.7 for completing the experiment and received an additional bonus payment of £0.77. Partial payments were made if the experiment was not completed due to technical issues ( $N = 6$ ) or early termination by the participant ( $N = 1$ ). Participants performing below 90% correct on catch trials ( $N = 19$ , 3 female, 16 male), or failing to respond in the allotted time window (15s) in more than 10 trials ( $N = 9$ , 4 female, 4 male, 1 diverse) were excluded. Thus, ( $N = 473$ ) participants remained in the dataset (202 female, 269 male, 2 diverse; mean age =  $31.82 \pm \text{SD} = 8.03$  years). Of these participants, ( $N = 448$ ) were each tested with a different selection of triplets, while ensuring that each triplet was presented  $N = 5$  times across the entire sample of participants (see information on stimuli sampling below). Due to a server glitch during trial assignment, the remaining ( $N = 25$ ) participants shared their exact triplet selection with one other participant in the sample. These ( $N = 25$ ) participants were excluded from the response times (RT) and uncertainty estimation (see Sec. 2.2.1) to restrict analysis to participants with different sets of triplets. The experiment was approved by the internal review board (IRB) of the Max Planck Institute for Human Development.

**Stimuli.** The experimental stimuli were images taken from the ImageNet dataset [Deng et al., 2009]. Another 9 images were used for instructions only and depicted natural objects selected from the Bank of Standardized Stimuli [BOSS; Brodeur et al., 2014], available at BOSS. We grouped the visual stimuli presented in the triplets according to different levels of abstraction: *coarse-grained semantic*, which comprised three images from three different categories; *fine-grained semantic*, showing three images from the same category; and *class-boundary*, where two images were from the same and one from a different category.

Instead of randomly sampling triplets—which would reproduce dataset biases—we stratified sampling by superclasses. ImageNet classes follow the WordNet hierarchy Deng et al. [2009]; Russakovsky et al. [2014], which includes higher-level classes. For instance, all dog breeds can be summarized as a single dog superclass. To avoid presenting dogs, birds, and other fine-grained classes that are overrepresented in ImageNet more frequently to the participants than other categories, we grouped the ImageNet classes into 717 coarse-grained WordNet superclasses. We uniformly at random sampled images from those 717 superclasses to construct the different kinds of triplets. Note that for all superclasses with more than one class, we uniformly at random chose one subclass and either uniformly at random sampled one image, two images (without replacement), or three images (without replacement) from that subclass, depending on the triplet type. For most superclasses that were comprised by a single subclass only, i.e., a *one-to-one-mapping*, we could skip the subclass sampling part. Triplet sampling resulted in ( $N = 450$ ) predefined experiment trial sets, of which ( $N = 448$ ) were used for testing. Across these, each triplet was presented within ( $N = 5$ ) different experiment files. This sampling process ensured a balanced distribution of triplets across the sample, and the repetition of each triplet in five different participants allowed for the calculation of an uncertainty distribution for each triplet.

**The triplet odd-one-out task.** On each trial, participants were presented with a triplet of images ( $i, j, k$ ). Participants were asked to select the image that was the most different from the other two, i.e., the odd-one-out. During the instructions, participants saw different triplets with increasing ambiguity regarding which image would likely be picked as the odd-one-out. Participants were given explanations for potential odd-one-out choices, clarifying that decisions could be based on different criteria, such as semantic or perceptual features of the shown images.

**Procedure.** The experiment was run online using `jsPsych v7.3.3` and custom plugins. Participants were asked to provide demographic information, including their age and gender. Thereafter, they viewed written instructions about the task and performed six practice trials (2 trials per triplet level of abstraction). Participants were free to repeat the instructions until they felt confident to perform the experiment. The experiment proper comprised  $N = 330$  experiment trials. Each trial started with a fixation cross (1s), followed by the presentation of a triplet (max. 15s). Participants were asked to select the “odd-one-out” using the right, left, or downward facing arrow keys on their keyboard. Responses could be entered between 1-15s after triplet onset, after which the next trial started. Trials in which participants failed to submit a response were rare ( $M = 0.27\%$  of trials;  $\min = 0.00\%$ ,  $\max = 6.06\%$ ). The serial order of triplet types (e.g., fine-grained or coarse-grained semantic) and ImageNet classes (e.g., dogs or birds) was counterbalanced across the experiment. We additionally counterbalanced the serial position of trial types across participants using a Latin-Square approach [LSD; Grant, 1948]. Participants could take short breaks (self-paced for up to 2 minutes) after  $N = 50$ ,  $150$ , and,  $200$  experiment trials; Experimental trials were interleaved with  $N = 16$  catch trials (class border triplets), which were predefined based on low model uncertainty and 100% agreement among participants on these specific triplets during piloting. Catch trial performance was used as an indicator of adequate task engagement (see participant inclusion criteria above).

**Preprocessing of human response times and uncertainty estimation.** Descriptive statistics on

response times (RT) and uncertainty estimation (see Sec. 2.2.1) were calculated based on participants with unique experimental trial sets ( $N = 448$ ). The RT data were log transformed ( $\log(\text{RT})$ ), in accordance with current best practices for RT analysis. Trials with RTs longer than 10 seconds were excluded from analysis (on average  $M = 2.64\%$  of trials per participant). Since responses could be given no earlier than 1 s after triplet onset (see *Procedure* above), no lower bound was set for RT-exclusion. To estimate uncertainty (in terms of the level of (dis-)agreement among observers) for each triplet, we used the discrete (Shannon) entropy of the response distribution across participants.

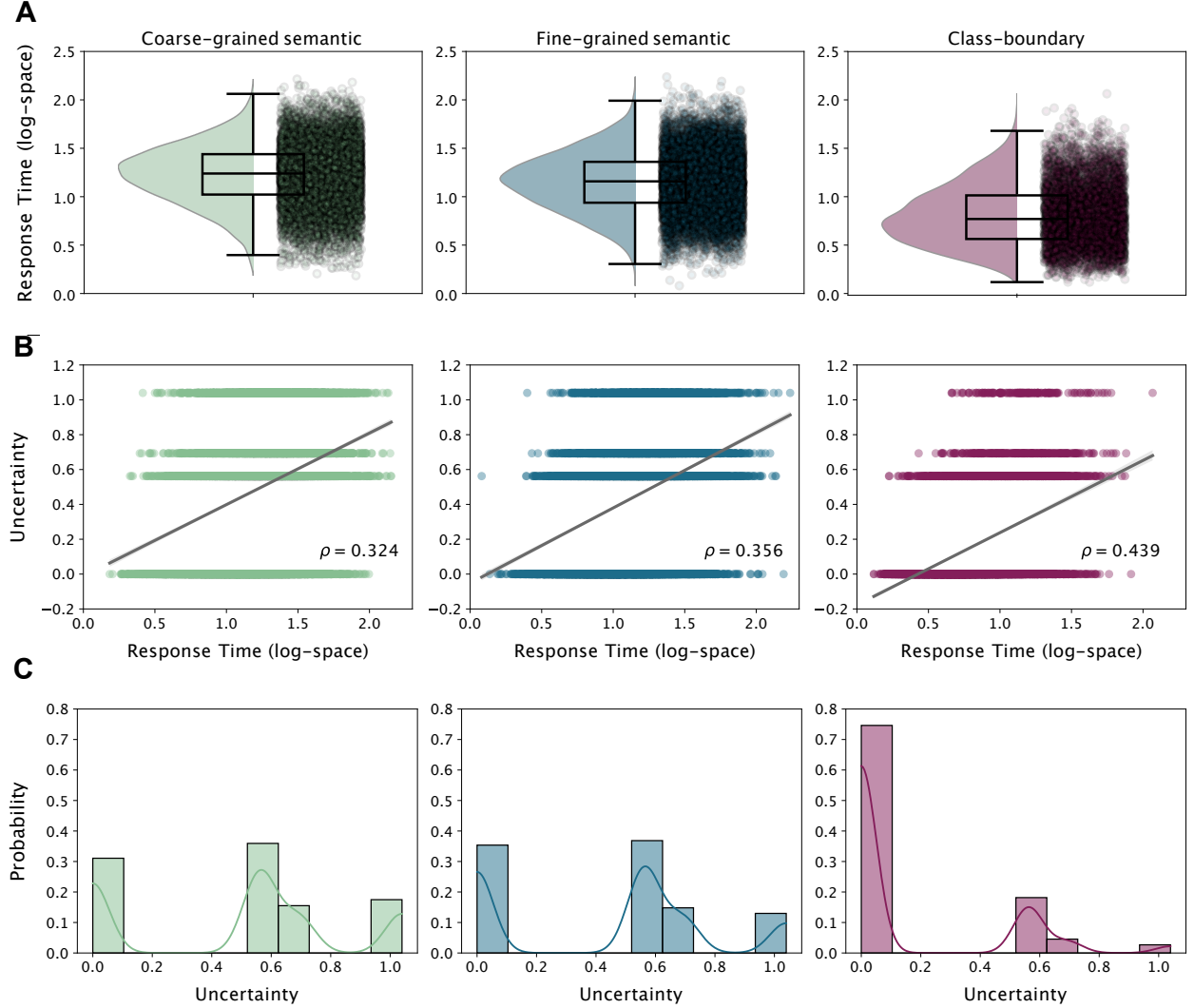


Figure 5 | Human response times and disagreement levels for the different triplet types. **A:** Distribution of human response times (in log-space) for the three different triplet type settings. **B:** Spearman rank correlation and linear regression fit of the participant disagreement levels/uncertainties with the participants' response times (measured in log-space). **C:** Probability distributions of the participant disagreement levels/uncertainties for the three triplet type settings.

## B. Additional/Detailed Results

In addition to the results that we presented in the main paper, here, we report the same set of results in more detail and add further analyses that we touched upon in the main part but did not go into much detail. We start by presenting findings from a comprehensive set of evaluations that we performed to test the alignment of model representations with human similarity judgments both for

similarity judgments collected in previous efforts [c.f. [Peterson et al., 2018](#); [Cichy et al., 2019](#); [King et al., 2019](#); [Hebart et al., 2020](#)] and for our own similarity judgment dataset Levels (see Section A.3). Subsequently, we demonstrate benefits of our method for machine learning downstream tasks that test generalization, such as *few-shot learning* and *out-of-distribution detection*. Finally, we perform a rigorous qualitative analysis of the changes in the model representations after applying our alignment framework to the various student models.

## B.1. Human Alignment

In this section, we present additional evaluation results regarding the alignment of model representations with human similarity judgments, complementing Sec. 2.2. For every student vision foundation model, we consider four settings of model representations and their refinements,

- *Original*: We use the pretrained representations of every student model without any changes to their representation space.
- *Distillation without alignment*: We perform AligNet fine-tuning without the first step (see Fig. 1) of aligning the teacher model with the human similarity judgments in THINGS. That is, we distill the teacher similarity structure of the pretrained, non-aligned SigLIP-So400m model (see Sec. A.1.4) into a student VFM.
- *Uncertainty Distillation (UD)*: We learn a linear transform of the models’ pretrained representation space into a human global object similarity space (using the THINGS triplet odd-one-out choices) while preserving the model’s local similarity structure (see Eq. 3). We remark that this does not involve any step of the AligNet framework. The weights of the student models are frozen during the UD optimization.
- *AligNet/Soft-alignment*: We learn a new representation space using the full AligNet framework as outlined in Sec. 4.1. This can be referred to as *soft-alignment*.

### B.1.1. Detailed results for RSA

In Tab. 1 we present the average alignment scores for all student models that we considered in our analyses (see Sec. A.1.5) and each of the four representation settings defined above for the datasets from [Cichy et al. \[2019\]](#), [King et al. \[2019\]](#), and [Hebart et al. \[2020\]](#). For the former two datasets, alignment is measured via RSA using Spearman rank correlation between the upper triangulars of the pairwise similarity matrices. For those datasets, human similarity judgments were collected using a multi-arrangement task where participants were asked to arrange (natural) objects on a computer screen (see Sec. A.2.1 for details). For the THINGS dataset, alignment is measured via triplet odd-one-out accuracy, i.e., the fraction of triplets for which models selected the same odd-one-out object as the human participants.

We find that base models—that is the *original* representation setting (see above)—performed poorly for almost every human similarity judgment dataset (see Tab. 1 and Fig. 6). The differences among the models in this setting is significant. While DINOv2 ViT-B achieves a Spearman rank correlation coefficient of  $\rho = 0.492$ ,  $p < 0.001$  for the dataset in [Cichy et al. \[2019\]](#) and an odd-one-out accuracy of 51.21% for the THINGS dataset, ViT-L is not correlated with the human similarity judgments from [Cichy et al. \[2019\]](#) and [King et al. \[2019\]](#) ( $\rho = 0.041$  and  $\rho = 0.095$  respectively) and shows a close to chance-level odd-one-out accuracy of 34.84% for the THINGS dataset (see Tab. 1 and x-axis in Fig. 7). AligNet fine-tuning significantly improved the alignment scores of all models for all datasets. In addition, it minimized the differences between the models to an extent that their differences in the degree of alignment are not statistically significant. Thus, AligNet fine-tuning models are equally well aligned with human similarity judgments irrespective of their architecture, pretraining data, and objective function.

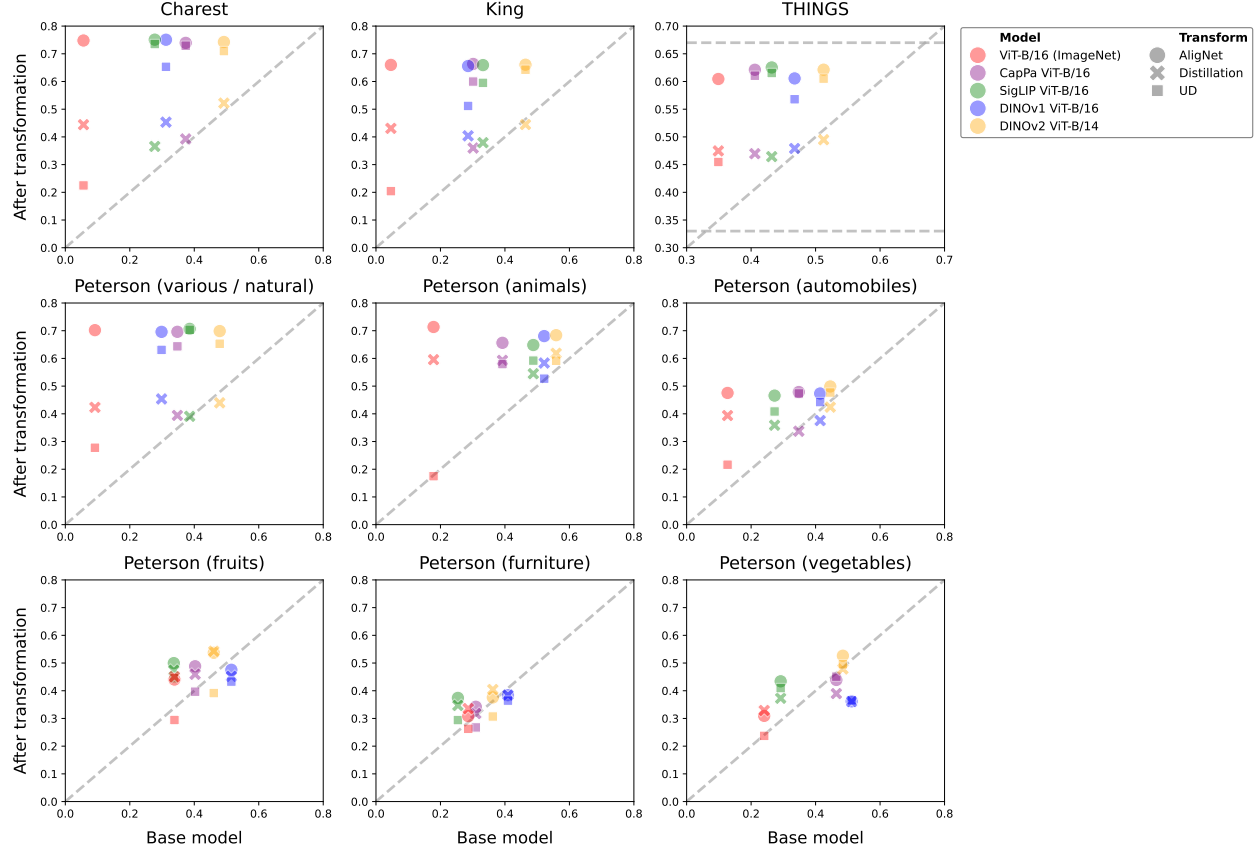


Figure 6 | Alignment of model representations with human similarity judgments for the four different representation settings *Original*, *Distillation*, *UD*, and *AligNet* for all models with a ViT-B backbone. The *x*-axis shows the degree of alignment for the base model, i.e., the *original* representations, whereas the *y*-axis displays the degree of alignment after linearly transforming the representations via *UD* or fine-tuning the models using distillation (without alignment) or the full *AligNet* framework. For all datasets but *THINGS* alignment is measured as the Spearman rank correlation coefficient between human and model RSMs. For *THINGS*, alignment is measured as triplet odd-one-out accuracy, i.e., the fraction of triplets for which models selected the same odd-one-out object as the human participants. Dashed horizontal lines for *THINGS* depict random guessing (0.333) and the human noise-ceiling/reliability score (0.667) respectively.

Model \ Fine-tuning	Cichy et al. [2019]				King et al. [2019]				Hebart et al. [2020]			
	Original	Distillation	UD	AligNet	Original	Distillation	UD	AligNet	Original	Distillation	UD	AligNet
ViT-S	0.083	0.520	0.367	0.743	0.143	<b>0.486</b>	0.353	<b>0.665</b> <sup>†</sup>	39.28%	<b>49.97%</b>	50.01%	59.44%
ViT-B	0.056	0.444	0.225	0.748	0.046	0.431	0.204	0.660	34.92%	47.47%	45.47%	60.45%
ViT-L	0.041	<b>0.540</b>	0.227	<b>0.751</b> <sup>†</sup>	0.095	0.463	0.201	0.664	34.84%	49.30%	44.40%	60.75%
CapPa ViT-B	0.373	0.393	0.729	0.739	0.301	0.360	0.599	0.663	40.58%	46.97%	61.04%	62.11%
DINOv1 ViT-B	0.312	0.453	0.653	<b>0.751</b> <sup>†</sup>	0.286	0.404	0.512	0.656	46.75%	47.91%	56.80%	60.56%
DINOv2 ViT-B	<b>0.492</b>	0.522	0.710	0.743	<b>0.464</b>	0.445	0.661	<b>51.24%</b>	49.49%	60.51%	62.13%	
SigLIP ViT-B	0.277	0.366	<b>0.735</b>	<b>0.751</b> <sup>†</sup>	0.332	0.379	0.595	0.659	43.20%	46.44%	61.53%	<b>62.54%</b> <sup>†</sup>
SigLIP So400m (Teacher)	0.226	–	0.723	–	0.267	–	<b>0.638</b>	–	44.24%	–	<b>61.70%</b>	–

Table 1 | Human alignment results for three different human similarity judgment datasets. The datasets from Cichy et al. [2019] and King et al. [2019] were collected using a multi-arrangement task. For those datasets, alignment with human similarity judgments is measured via RSA using the Spearman rank correlation. The dataset from Hebart et al. [2020] used a triplet odd-one-out task for collecting human judgments. Here, alignment with human choices is measured via triplet odd-one-out accuracy (%). Bold face indicates highest performance within a single column and <sup>†</sup> indicates best performance for a dataset overall.

In the top row of Fig. 6 we show the performance of the transformed representations as a function

of the base model performance for those datasets. We can see that AligNet fine-tuning significantly improves upon the base model representations ( $x$ -axis). It yields the most human-aligned models across all three datasets (depicted by the circles) and often substantially improves upon the linearly aligned representations (depicted by the squares).

Model \ Fine-tuning	Peterson et al. [2016, 2018] (coarse-grained)				Peterson et al. [2016, 2018] (fine-grained)			
	Original	Distillation	UD	AligNet	Original	Distillation	UD	AligNet
ViT-S	0.249	<b>0.454</b>	0.379	0.663	0.330	0.461	0.320	0.459
ViT-B	0.092	0.423	0.278	0.702	0.234	0.421	0.237	0.449
ViT-L	0.118	0.448	0.231	0.704	0.221	0.421	0.234	0.447
CapPa ViT-B	0.347	0.394	0.644	0.696	0.383	0.419	0.434	0.481
DINOv1 ViT-B	0.299	<b>0.454</b>	0.631	0.696	<b>0.474</b>	0.431	0.426	0.475
DINOv2 ViT-B	<b>0.479</b>	0.440	0.653	0.699	0.462	<b>0.494</b>	<b>0.452</b>	<b>0.524</b> <sup>†</sup>
SigLIP ViT-B	0.386	0.391	<b>0.703</b>	<b>0.707</b> <sup>†</sup>	0.329	0.419	0.430	0.484

Table 2 | Human alignment results for the dataset from Peterson et al. [2016, 2018]. Human pairwise similarity judgments were collected using an ordinal Likert scale. Scores reflect the average Spearman rank correlation coefficients with the human pairwise similarity judgments. To obtain an average alignment score for the fine-grained setting, we averaged the performances across the five single category settings: animals, automobiles, fruits, furniture, and vegetables. Bold face indicates highest performance within a single column and <sup>†</sup> indicates best performance for a dataset overall.

Human similarity judgments from the dataset introduced in Peterson et al. [2016, 2018] were collected using an ordinal Likert scale (see Sec. A.2.2 for details). The authors collected pairwise similarity ratings for various natural objects with one image per category, similar to the other three human similarity judgment datasets. Thus, those pairwise similarity ratings reflect global **coarse-grained** semantic structure. In addition, the authors collected pairwise similarity ratings for multiple images from a single category that reflect local **fine-grained** semantics. The specific categories for which similarity ratings were collected are animals, automobiles, fruits, furniture, and vegetables. We average model performances across those five single category pairwise similarity rating datasets to obtain a single measure for fine-grained semantic and refer to it as the fine-grained dataset of Peterson et al. [2016, 2018]. In Tab. 2, we report Spearman rank correlation coefficients of the model RSMs with the RSMs obtained from the human similarity ratings for all student models and the four representation settings. AligNet fine-tuning significantly improves performance across the board, even for the fine-grained setting. While the best model for the coarse-grained setting is AligNet fine-tuned SigLIP ViT-B ( $\rho = 0.707, p < 0.001$ ), AligNet fine-tuned DINOv2 ViT-B is most human-aligned model for the fine-grained setting ( $\rho = 0.524, p < 0.001$ ). AligNet fine-tuning significantly improves the Spearman rank correlation coefficients for all models compared to their original representations in the coarse-grained setting.

In the bottom two rows of Fig. 6 and Fig. 7 respectively we show model performances individually for the single category pairwise similarity rating datasets. We observe that AligNet fine-tuning significantly improved the degree of alignment for all models for the various, animals, and automobiles categories but there does not appear to be a difference in performance between the different model transformation settings for the categories fruits, furniture, and vegetables. We hypothesize that this difference in alignment benefits stems from the fact that animal- and automobile-related concepts are more frequently represented in the THINGS dataset than fruits-, furniture-, and vegetable-related concepts [c.f. Hebart et al., 2019, 2020]. Moreover, THINGS is a human similarity judgment dataset that reflects global coarse-grained semantic, similar to the coarse-grained setting in Levels. Thus, it is rather surprising to find benefits for human local fine-grained semantic by either UD or fine-tuning on AligNet.

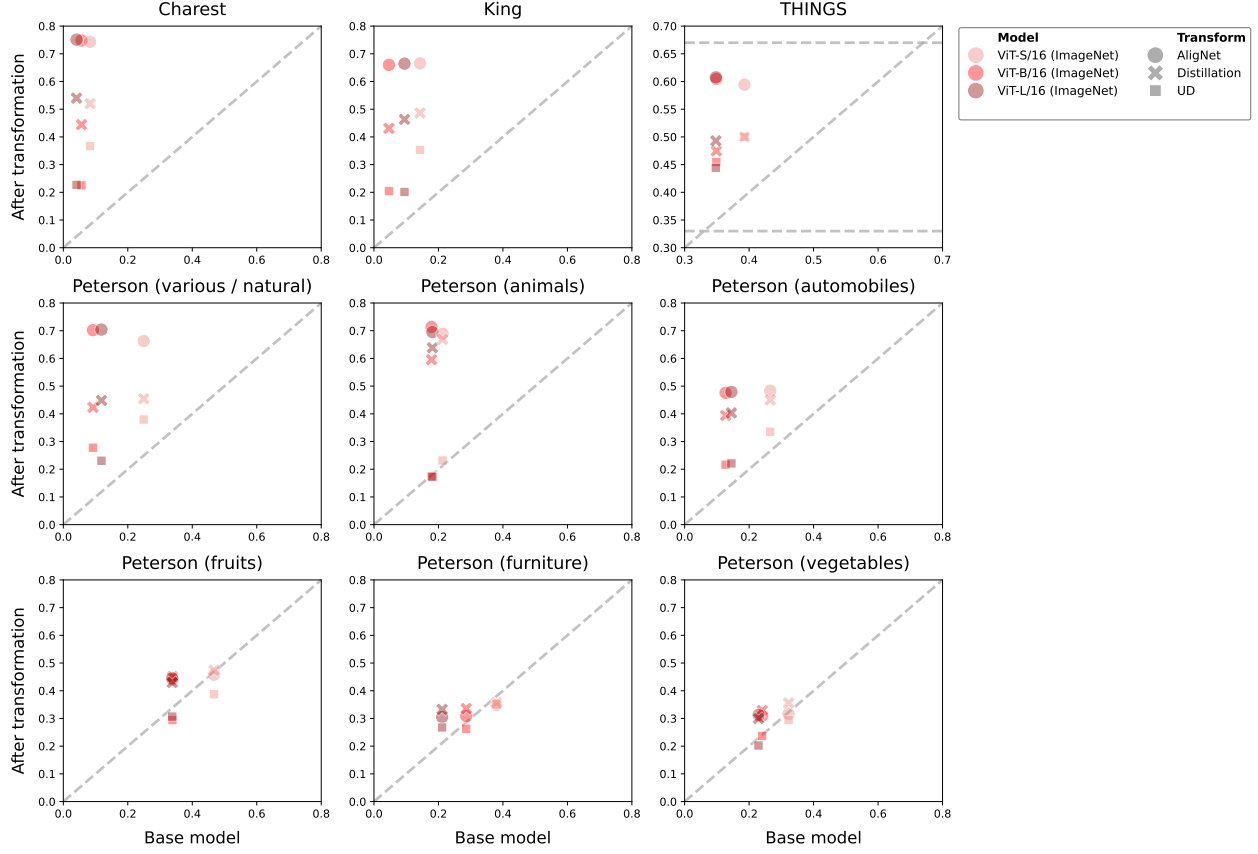


Figure 7 | Alignment of model representations with human similarity judgments for the four different representation settings *Original*, *Distillation*, *UD*, and *AligNet* for the three supervised ImageNet-trained ViT models. The  $x$ -axis shows the degree of alignment for the base model, i.e., the *original* representations, and the  $y$ -axis displays the degree of alignment after linearly transforming the representations via *UD* or fine-tuning the models using distillation (without alignment) or the full *AligNet* framework. For all datasets but THINGS alignment is measured as the Spearman rank correlation coefficient between human and model RSMs. For THINGS, alignment is measured as triplet odd-one-out accuracy, i.e., the fraction of triplets for which models selected the same odd-one-out object as the human participants. Dashed horizontal lines for THINGS depict random guessing (0.333) and the human noise-ceiling (0.667) respectively.

### B.1.2. Larger models benefit more from *AligNet*

In Fig. 7 we compare supervised ImageNet-trained ViTs of different sizes. Interestingly, the smallest version of the ViTs, ViT-S, achieved the best base model performance across the board. That is, their original representation space was better aligned with the different human similarity judgments than the representation spaces of the larger ViT backbones (see Fig. 7 and Tables 1, 2). However, after fine-tuning the models on *AligNet* the larger ViT versions were either better or equally-well aligned than ViT-S.

### B.1.3. Detailed results for Levels

In Tab. 3 we present triplet odd-one-out accuracies for every model that we considered in our analyses for each of the three levels of abstraction in the Levels dataset.

**Global coarse-grained.** In this setting, *AligNet* fine-tuning improved alignment with human similarity judgments most significantly. Before fine-tuning, models achieved poor odd-one-out accuracies of

35.45% (ViT-L) – 57.38% (DINOv2 ViT-B). Fine-tuning models on AligNet closed this gap and significantly improved the alignment between human and model responses to the extent that all models performed with odd-one-out accuracies of 65.70% (DINOv1 ViT-B) – 68.60% (ViT-L) above the human-to-human reliability score of 61.92%. Interestingly, the most poorly performing model before fine-tuning, ViT-L, achieved the highest odd-one-out accuracy after fine-tuning on AligNet, with a relative improvement of almost 93.51%. Even the worst performing AligNet-tuned model, DINOv1 ViT-B, performed with an odd-one-out accuracy of 65.70% significantly better than the best performing base model, DINOv2 ViT-B with 57.38%, and better than the best performing model after vanilla distillation without alignment, ViT-S with 58.82%, (see the *coarse-grained* column in Tab. 3). The relative performance improvements ranged from 19.48% (DINOv2 ViT-B) – 93.51% (ViT-L). Three models—SigLIP ViT-B, DINOv2 ViT-B, and ViT-L—performed even better than the teacher model which is the strongest baseline in that setting that exists at the time of writing this manuscript.

**Local fine-grained.** The responses of most base models’ did not strongly correspond to human responses for fine-grained semantics either and, thus, model performances were far from the human reliability score. The human noise-ceiling was with 65.92% similar to the noise-ceiling of the coarse-grained setting. Prior to fine-tuning, models achieved poor alignment scores of 40.75% (ViT-L) – 57.72% (DINOv2 ViT-B), except for DINOv1 ViT-B whose base model performance (62.92%) was significantly better than the performance of the other models (see Tab 3).

Soft-alignment improved this mismatch to some degree but not as significantly as it did for the coarse-grained abstraction setting. AligNet models achieved odd-one-out accuracies of 58.93 (ViT-S) – 62.92% (DINOv1 ViT-B) (see the *fine-grained* column in Tab. 3). Here, relative increases in performance ranged from 7.84% (DINOv2 ViT-B) - 46.03% (ViT-L). For a single model, DINOv1 ViT-B, the alignment score did not change after soft-alignment. Again, the best performing soft-aligned model, DINOv1 ViT-B, performed with an odd-one-out accuracy of 62.92% better than any other model—whether linearly aligned using UD or fine-tuned via teacher distillation—in that setting. Note that UD and fine-tuning via distillation decreased the performance of DINOv1 ViT-B. This model performed closest to the human reliability score of 65.92%. Every soft-aligned model performed better than the teacher in that abstraction setting.

It is rather surprising that AligNet models were better aligned than their base models for this setting because the THINGS triplets reflect coarse-grained semantic structure and, hence, neither teacher nor student representations have ever explicitly learned anything about a fine-grained human object similarity space. We hypothesize that the fusion of information about human coarse-grained semantic and the teacher model’s local similarity structure leads to a representation space that better reflects human object similarity structure in general—irrespective of the level of granularity.

**Class-boundary.** Supervised classifiers and image/text contrastive models performed close to the noise ceiling for class-boundary triplets prior to any fine-tuning. Their odd-one-out accuracies ranged from 81.96% (SigLIP ViT-B) to 93.67% (ViT-L) (see Tab. 3). However, the caption generator model (CapPa) often responded differently from the human participants in that setting and achieved a significantly lower odd-one-out accuracy score compared to the other student models. It selected the same odd-one-out image as the human participants in 70.37% of the triplets.

AligNet fine-tuning changed the representation spaces of all models to be equally well aligned with the human respondents. The differences between AligNet models was significantly smaller compared to the other settings, with odd-one-out accuracies of 93.09% – 94.24%. Surprisingly, the odd-one-out accuracies of models fine-tuned on AligNet were higher than the human reliability score of 89.21% (see Fig. 2D, rightmost column) with the best model achieving an impressive alignment score of 94.24% (ViT-L). This means that the responses of AligNet models were more similar to the average human responses—since each triplet response is the majority response of the subject

population—than the level of agreement among the human subjects themselves. The performances of all models improved by fine-tuning them on AligNet. The relative increases in performance were between 0.62% – 32.39%.

Simply performing *distillation without alignment* did not improve the models’ alignment with humans as significantly. For some models (e.g., ViT-L) simply distilling the similarity structure of the teacher model into the student without aligning the teacher’s representations even decreased the degree of alignment with the human odd-one-out responses (see the *class-boundary* column in Tab. 3). Similarly, applying the UD transformation to a model’s representation space sometimes slightly improved the human-model fit (e.g. ViT-B) and sometimes significantly decreased model performance (e.g. ViT-S) with large differences between models. Moreover, AligNet fine-tuning was the only transformation technique that could significantly decrease the variance in performance across the different student models. The difference between the worst (CapPa ViT-B) and the best (ViT-L) AligNet fine-tuned model was just 1.15%

Model \ Fine-tuning	Coarse-grained				Fine-grained				Class-boundary			
	Original	Distillation	UD	AligNet	Original	Distillation	UD	AligNet	Original	Distillation	UD	AligNet
ViT-S	40.08%	<b>58.82%</b>	46.29%	67.09%	51.30%	58.80%	43.41%	58.93%	92.23%	92.64%	85.31%	93.80%
ViT-B	36.10%	56.15%	40.96%	67.72%	46.04%	57.04%	42.66%	60.02%	88.73%	91.68%	<b>93.31%</b>	93.99%
ViT-L	35.45%	57.75%	41.84%	<b>68.60%<sup>†</sup></b>	40.75%	57.47%	39.34%	59.51%	<b>93.67%</b>	<b>93.18%</b>	<b>93.31%</b>	<b>94.24%<sup>†</sup></b>
CapPa-B ViT-B	42.99%	53.55%	66.73%	66.06%	49.36%	57.15%	53.07%	60.21%	70.37%	90.85%	87.92%	93.09%
DINOv1 ViT-B	52.44%	55.86%	57.82%	65.70%	<b>62.92%<sup>†</sup></b>	<b>59.76%</b>	<b>60.91%</b>	<b>62.92%<sup>†</sup></b>	90.09%	92.39%	88.84%	94.03%
DINOv2 ViT-B	<b>57.38%</b>	49.37%	66.09%	68.56%	57.72%	55.31%	55.72%	62.24%	89.74%	88.46%	90.13%	93.45%
SigLIP ViT-B	46.88%	51.72%	<b>68.17%</b>	68.47%	53.44%	57.39%	57.71%	60.94%	81.96%	90.81%	91.32%	93.75%
SigLIP So400m (Teacher)	50.24%	–	68.03%	–	57.27%	–	58.86%	–	90.42%	–	93.11%	–

Table 3 | Human alignment results for Levels. Here, we show triplet odd-one-out accuracies (in %)—measured as the fraction of triplets for which models selected the same odd-one-out image as the majority of the human participants for the three levels of abstraction—*coarse-grained*, *fine-grained*, and *class-boundary*—in the Levels dataset that we collected via online crowdsourcing. Bold face indicates highest performance within a single column and <sup>†</sup> indicates best performance for a triplet type setting overall.

#### B.1.4. Correlation of model output uncertainties with human RTs

Here, we evaluate how the uncertainties of the model outputs—measured as the discrete Shannon entropy of the triplet probabilities—correlate with the human response times for the different triplets. For all base models, we observed a poor (close to zero) Spearman rank correlation between its output uncertainties over the triplet odd-one-out choices and the human response times for both the global coarse-grained and the local fine-grained semantic settings (see panel A in Fig. 8). However, except for ViT-B and ViT-L, most base models showed a medium positive Spearman rank correlation ( $\rho=0.3\text{--}0.4$ ) for the class-boundary setting (see rightmost column in panel A Fig. 8). Note that the class-boundary setting is the easiest setting with the least variance/disagreement among the human participants (see Sec. A.3 for details). AligNet-finetuning significantly improved the correspondence between model output uncertainties and human response times for all models and triplet type settings. The improvements were most striking for the global coarse-grained semantic setting where every model achieved a medium to strong positive Spearman rank correlation of close to  $\rho=0.4$ . For the class-boundary setting, models fine-tuned on AligNet even achieved a strong positive Spearman rank correlation coefficient of close to  $\rho = 0.5$ .

In panel B of Fig. 8, we compare AligNet fine-tuned representations (darker colors) against performing distillation without alignment (lighter colors). We can see that simply performing distillation without alignment could improve the correspondence of model uncertainties and human response times over the base representations but the improvement was not as substantial compared to applying the full AligNet framework. We find that for every model and every triplet setting, AligNet fine-tuning yielded a significantly stronger Spearman rank correlation coefficient. In Fig. 9, Fig. 10, and

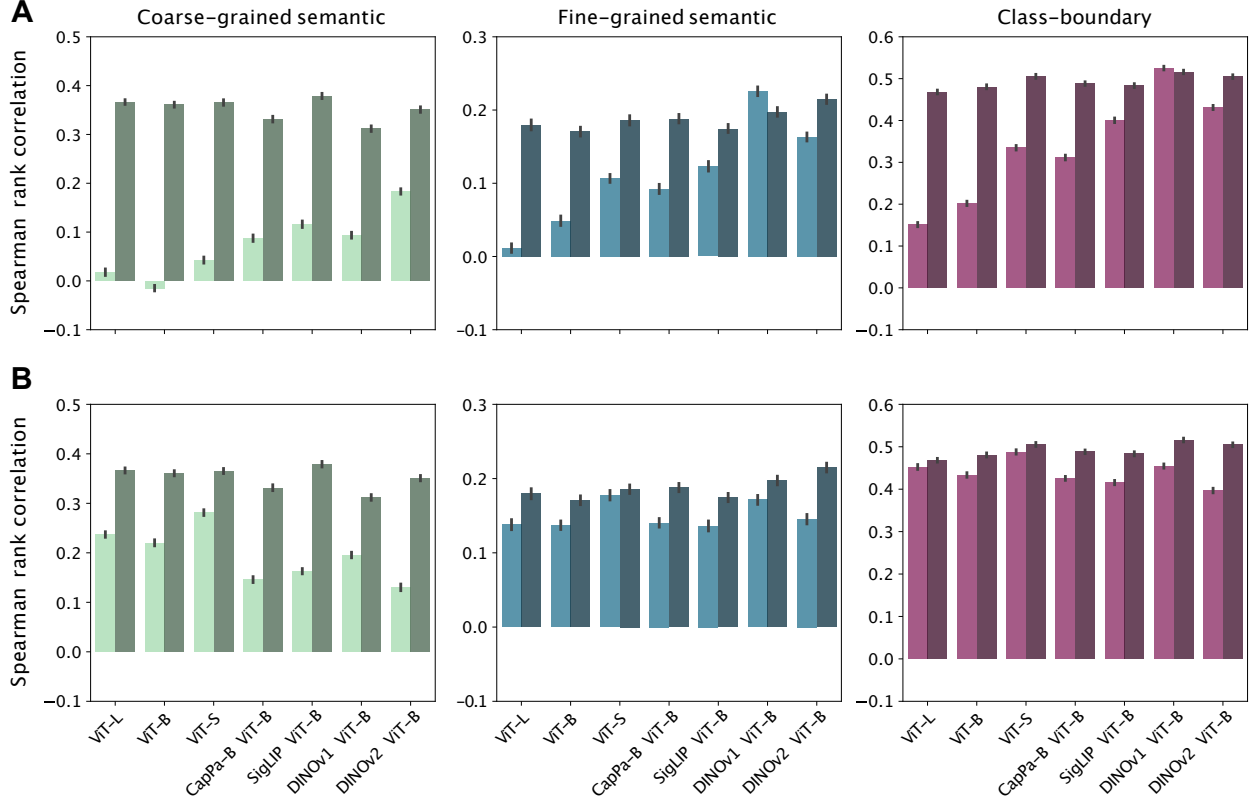


Figure 8 | Spearman rank correlation coefficients of model output uncertainties over the triplet odd-one-out choices (measured as discrete Shannon entropy) and the corresponding human response times (measured in log-space). The columns are partitioned into the three different triplet types: **coarse-grained**, **fine-grained**, and **class-boundary**. **A:** AligNet fine-tuning (darker colors) in contrast to the base model representations (lighter colors). **B:** AligNet fine-tuning (darker colors) in contrast to distillation without alignment (lighter colors). Error bars reflect the standard deviation (SD) on the item level over 1000 bootstraps.

Fig. 11 we contrast the human response times (in log-space) against the model’s output uncertainties over the triplet odd-one-out responses for ViT-B, DINOv2 ViT-B, and SigLIP ViT-B respectively for each triplet individually. We chose those three models because they reflect a representative subset of the student models (see Sec. A.1.5 that we fine-tuned on AligNet. Each of those models has the same backbone but was pretrained on a different datasets with a different objective function. We observe that AligNet fine-tuning significantly improved the correspondence of the models’ output uncertainties to the human responses times for all three models and triplet settings. Interestingly, distillation without alignment, decreased the Spearman rank correlation coefficient of DINOv2 for each of the three triplet settings (see panel B in Fig. 10). That was not the case for ViT-B and SigLIP ViT-B (see panel B in Fig. 9 and Fig. 11 respectively).

Taken together, we find that AligNet fine-tuning significantly improved the correspondence of models’ output uncertainties with the human response times irrespective of the task and objective with which a model was (pre-)trained and regardless of the specific triplet type. The improvements were most striking for global coarse-grained semantic.

## B.2. Machine Learning

In this section we provide further details and evidence about the machine learning downstream task performances of our method. We start by demonstrating few-shot learning and out-of-distribution

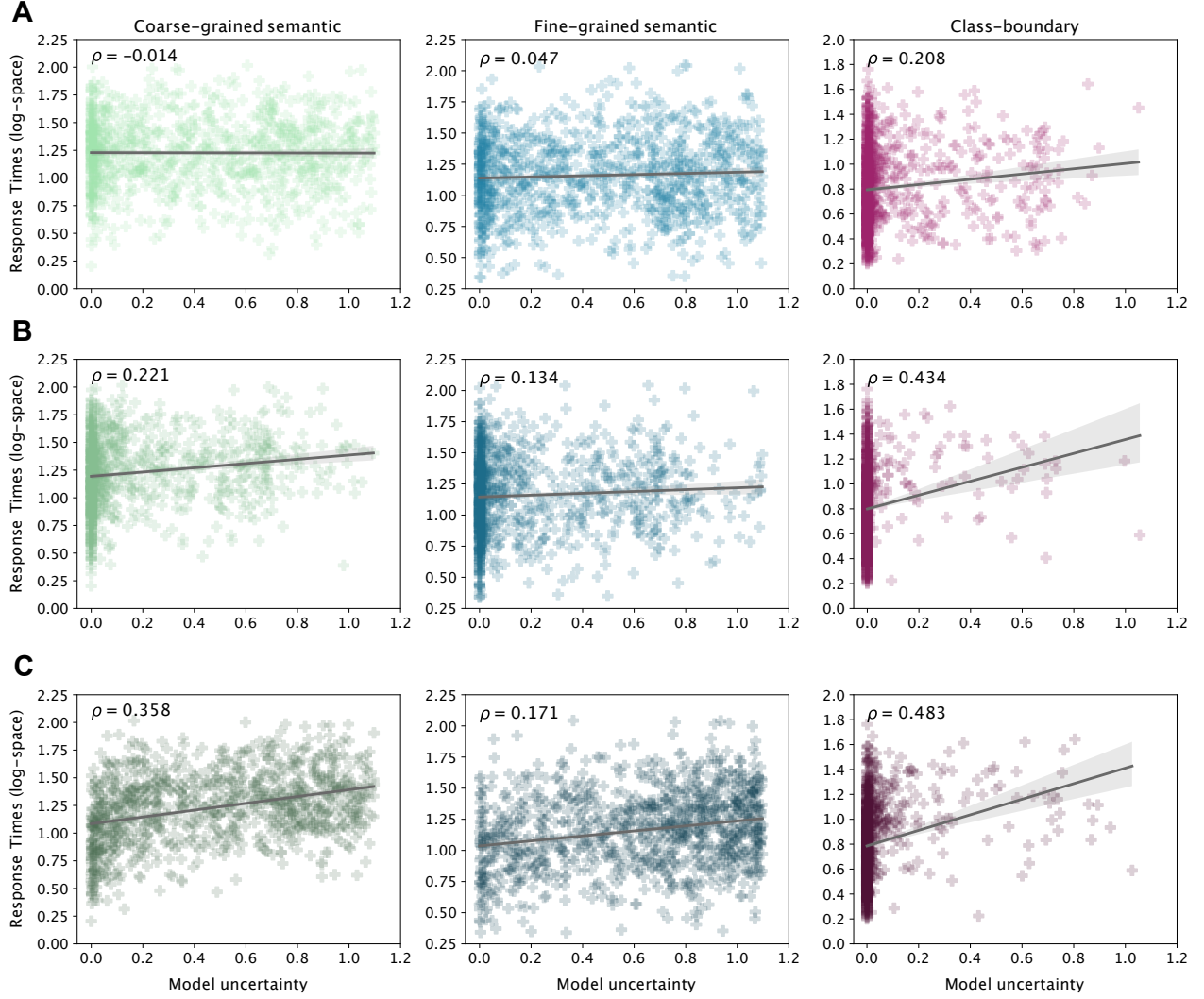


Figure 9 | Human response times (in log-space) as a function of ViT-B’s output uncertainty over the triplet odd-one-out choices (measured as the discrete Shannon entropy). The columns are partitioned into the three different triplet types: **coarse-grained**, **fine-grained**, and **class-boundary**. **A**: Model uncertainties of *original* representations. **B**: Model uncertainties of *distilled* representations. **C**: Model uncertainties of *AligNet-finetuned* representations. Correlation coefficients are Spearman rank correlations.

detection evaluations and end the section with showing various ablations.

### B.2.1. Few-shot learning

Few-shot learning [Wang et al. \[2021\]](#) is a common way to evaluate how easily a neural network representation can generalize to new tasks: The goal here is to learn a new task/dataset from very few labelled examples (typically  $\leq 10$  examples per labelled class), and then evaluate its performance on the full test set of that task. Good few-shot performance is indicative of models that have a solid understanding of many varying concepts, and that their representation is able to quickly integrate/expand to new or related concepts.

We run few-shot learning evaluations on eight different supervised tasks. ImageNet [[Russakovsky et al., 2014](#)], Places365 [[Zhou et al., 2018](#)] and Cifar100 [[Krizhevsky, 2009](#)] test for broad understanding of a wide variety of visual concepts, and gauge how easily a representation can adapt to

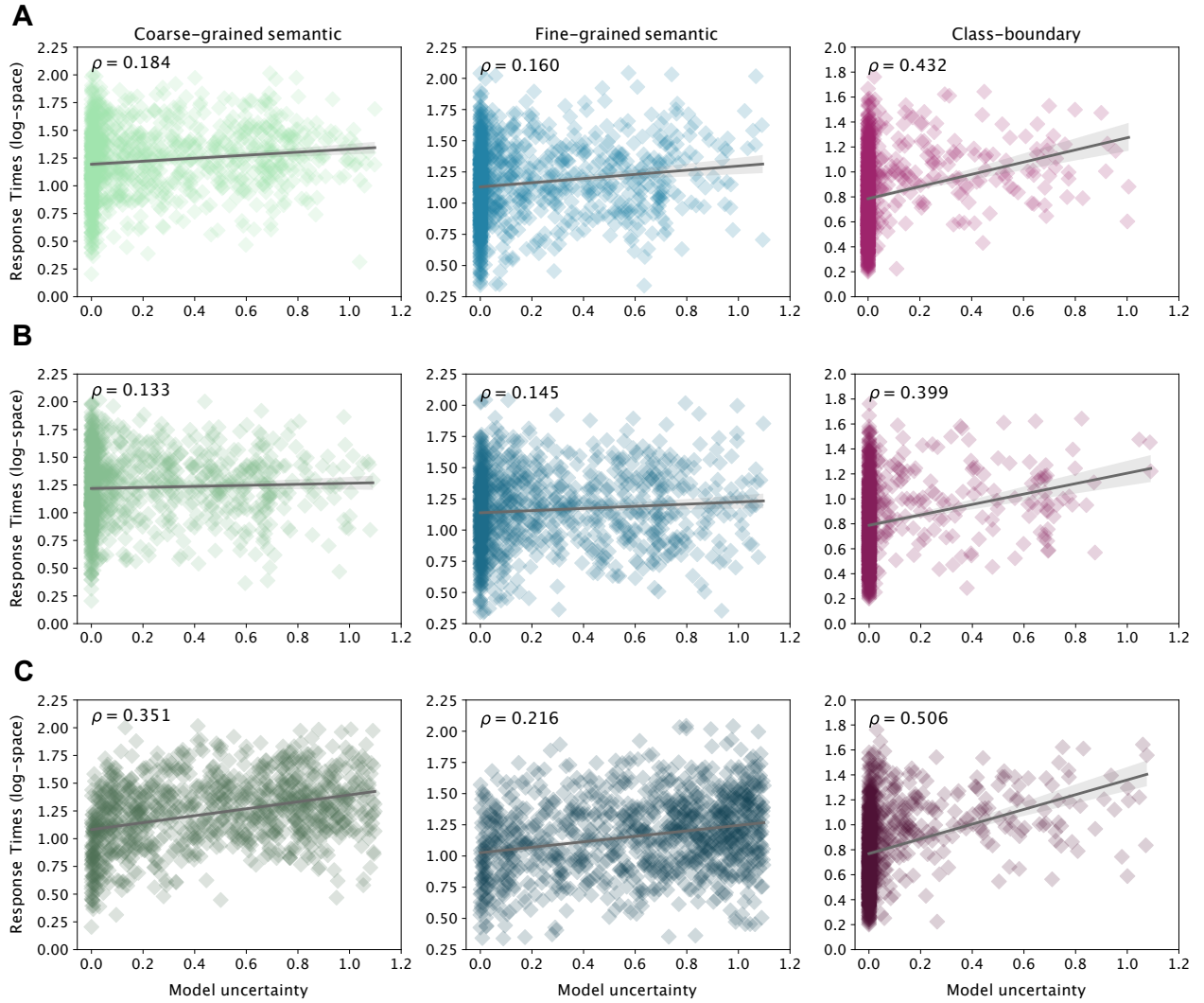


Figure 10 | Human response times (in log-space) as a function of DINOv2’s output uncertainty over the triplet odd-one-out choices (measured as the discrete Shannon entropy). The columns are partitioned into the three different triplet types: **coarse-grained**, **fine-grained**, and **class-boundary**. **A**: Model uncertainties of *original* representations. **B**: Model uncertainties of *distilled* representations. **C**: Model uncertainties of *AligNet-finetuned* representations. Correlation coefficients are Spearman rank correlations.

a new learning task on concepts a (pretrained) model has likely encountered before. We also test datasets that instead require that the model is able to differentiate between very fine-grained differences in related concepts. Concretely, we test datasets such as Caltech-UCSD Birds 200 (CUB-200) Birds [Welinder et al., 2010], Stanford Cars [Krause et al., 2013], Flowers [Nilsback and Zisserman, 2008], Oxford-IIIT Pets [Parkhi et al., 2012] and the UC Merced Land Use Dataset Yang and Newsam [2010]. For our tests, we freeze the model, and train a linear classifier on top of the extracted image representation Alain and Bengio [2016]. On all datasets, we test two few-shot settings: the extreme case where only a single example per class is provided (“1-shot”) and the more conservative, but still challenging ‘10-shot’ challenge.

In Fig. 12, we compare the few-shot performance of pre-trained models vs. their few-shot performance after being aligned-finetuned. AligNet finetuning is clearly beneficial on most datasets in both 1-shot and 10-shot evaluations. Even models that have previously been trained on ImageNet

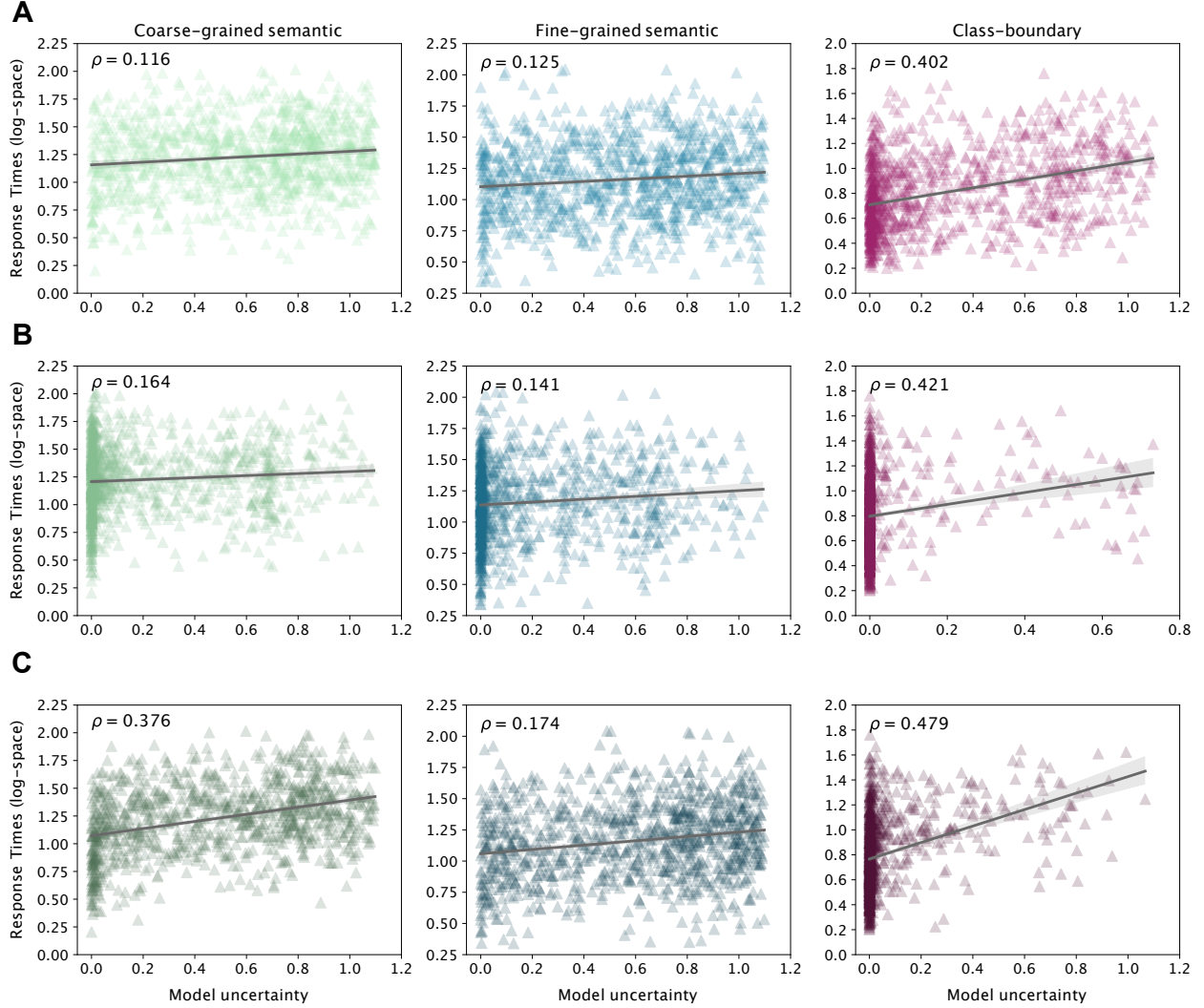


Figure 11 | Human response times (in log-space) as a function of SigLIP ViT-B’s output uncertainty over the triplet odd-one-out choices (measured as the discrete Shannon entropy). The columns are partitioned into the three different triplet types: **coarse-grained**, **fine-grained**, and **class-boundary**. **A**: Model uncertainties of *original* representations. **B**: Model uncertainties of *distilled* representations. **C**: Model uncertainties of *AligNet-finetuned* representations. Correlation coefficients are Spearman rank correlations.

data (e.g. DINOv1 ViT-B/16 and supervised ViT-B/16) show improvements on 1-shot ImageNet performance, which indicates that the benefits do not merely come from being exposed to ImageNet data, but also from the label information we distilled into AligNet.

### B.2.2. Out-of-distribution

In this section we investigate the how robustly a neural network has learned visual concepts: how well can they recognize objects under different, more challenging settings? This is an important question for many applications, and gives an idea both of the generalization properties, as well as to the practical applicability of models. To investigate robustness, we look at six different out-of-distribution testsets for the popular ImageNet dataset in Fig. 13. ImageNet ReAL [Beyer et al., 2020] relabels the dataset to fix inaccuracies/oversights in the original data. ImageNet V2 [Recht et al., 2019] is a new, updated test-set for the original dataset. ImageNet-A [Hendrycks et al., 2021b] consists of adversarial

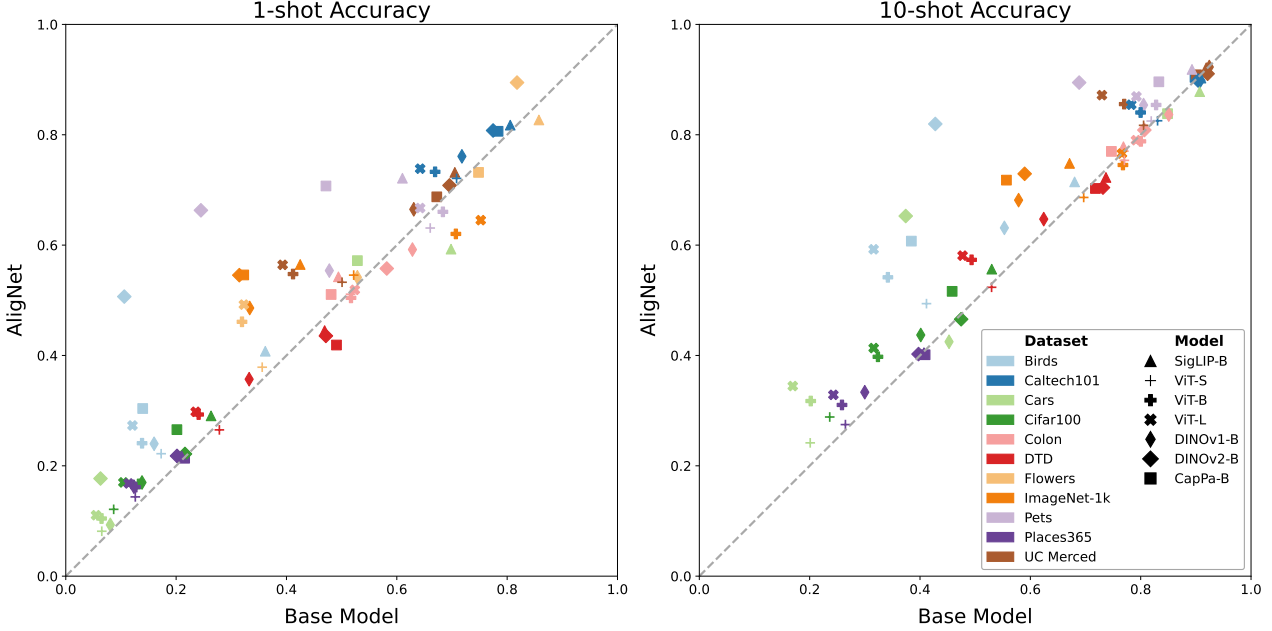


Figure 12 | Results for 1-shot and 10-shot linear probing on a number of common few-shot evaluation datasets.

examples, whose aim is to confuse/trick modern systems. ImageNet-C [Hendrycks and Dietterich, 2019] tests how well models can deal with corrupted inputs, e.g. very noisy or blurry images. Finally, ImageNet-R [Hendrycks et al., 2021a] shows more abstract renditions of actual objects, for example sketches, sculptures or drawings.

As we see in the results, AlignNet finetuning has a positive impact on the models under investigation, with most datasets showing slight improvements. On average over all models and across all datasets, accuracy went up by 2.6 percentage points, which on Imagenet-like datasets is considered a large performance boost [Beyer et al., 2020]. As can be expected, the models that were pre-trained on imangenet already showed the smallest improvements. Even on ImageNet ReAL, which can be considered a more reliable measure of model improvement than the original Imagenet, on average the models improved by 1.5%. The clearest advantage of AlignNet can be seen for adversarial examples where AlignNet-finetuned models exhibit much better behavior than their baseline counterparts: the average improvement was a jump of 5.6 percentage points. For corruptions and renditions, the situation is mixed: while on average the results still show an improvement of 1.8% on ImageNet C and 1.4% on ImageNet R, the SigLIP models slightly deteriorated. Overall, this fits with our understanding of what AlignNet is meant to achieve: it allows models to learn clearer concepts that generalize better, but it is not improve performance in situations where image corruption or artistic renditions are the cause of misclassifications.

### B.2.3. Ablations

We performed several ablations to see how the AlignNet procedure changes if we modify some of its crucial parameters.

**Model Capacity** To investigate if AlignNet finetuning affects models of different capacity the same way, we compared the performance on the ViT-B model (87M parameters) with a smaller ViT-S (22M parameters) and a larger ViT-L (305M parameters) model. The results in Fig. 12 and Fig. 13 indicate that the positive impact of AlignNet increases with model scale. For example, the average 10-shot performance improved by 2.4% points for ViT-S, by 6.3% points for ViT-B and by 8.3% points for

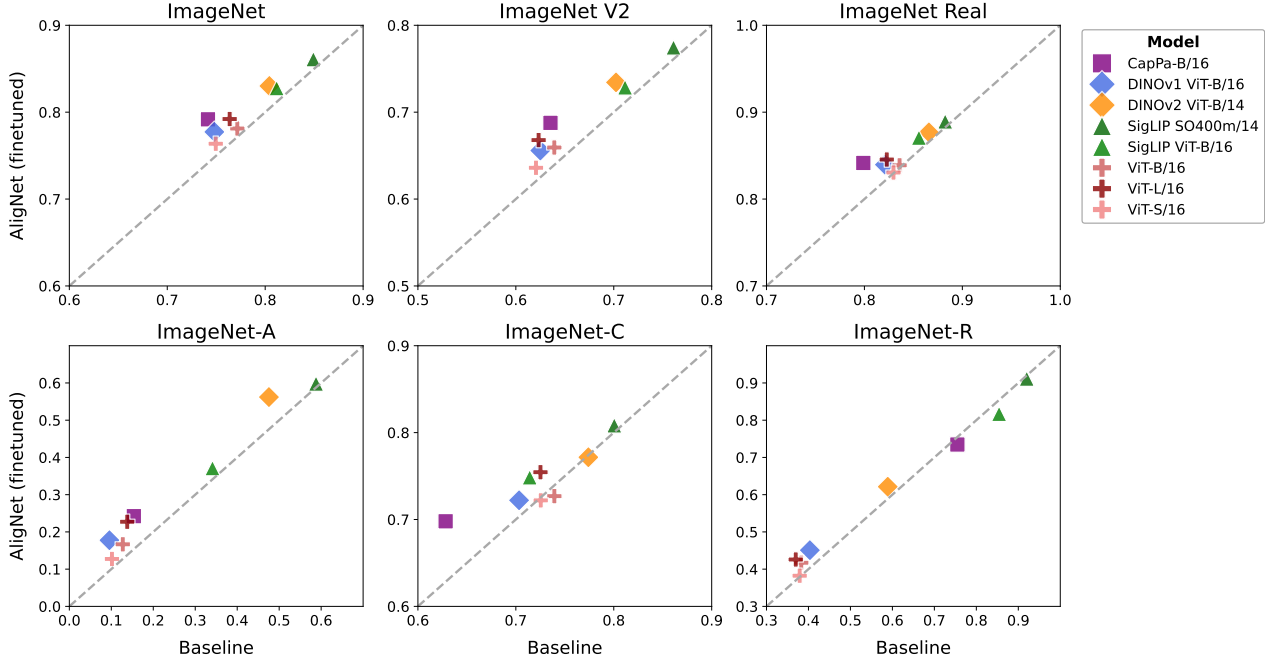


Figure 13 | Out of distribution results on variations of ImageNet.

ViT-L. Similar results hold up for all datasets we investigated. Our hypothesis is that the larger model capacity afford the model to better absorb the additional high-level information provided by the human similarity judgments distilled into AligNet.

**Increasing the Number of Images or Triplets** We also wanted to see how AligNet scales with the amount of available training data. We individually varied the number of ImageNet images we used to construct our dataset over 3 orders of magnitude, and the number of triplets that we sampled across 4 orders of magnitude. We then looked at the 1-shot results across all the few-shot datasets described in Appendix B.2.1 (Outcomes for 10-shot were not qualitatively different). The results in Fig. 14a show that AligNet performance only increases slightly as the number of available base images increases. However, as we can see from Fig. 14b, the number of generated triplets does influence the outcome, though we hit diminishing returns eventually. We do not expect to be able to increase AligNet performance much further by simply increasing the amount of available data.

**Using an Unaligned Teacher Model** An important part of the AligNet pipeline is to align the teacher model to human similarity judgments using a specially trained affine transformation. Here we investigate the effect of this step, by generating a variant of AligNet without this transformation that we call UnAligNet. For this dataset we do not use any human odd-one-out data, so finetuning on UnAligNet is equivalent to distilling the teacher model using our triplet sampling procedure. Fig. 15A compares the odd-one-out accuracy of various student models when fine-tuning on AligNet vs on UnalignedNet. As expected, we find that using an unaligned teacher leads to substantially worse alignment of the student models. Though it should be noted that some models (especially the ViTs trained on ImageNet) can already profit even from an unaligned teacher.

It is perhaps unsurprising that an aligned teacher improves the alignment of the student models. A more interesting question is, whether an aligned teacher also improves the students performance on other tasks such as few-shot classification. Fig. 15B thus compares 1-shot performance after training on UnalignedNet (x-axis) with performance after training on AligNet (y-axis). The first thing to note here, is that the differences between AligNet and UnalignedNet are much smaller than the differences between AligNet and the Base Model (cf. Fig. 12). This shows that the few-shot improvements are in

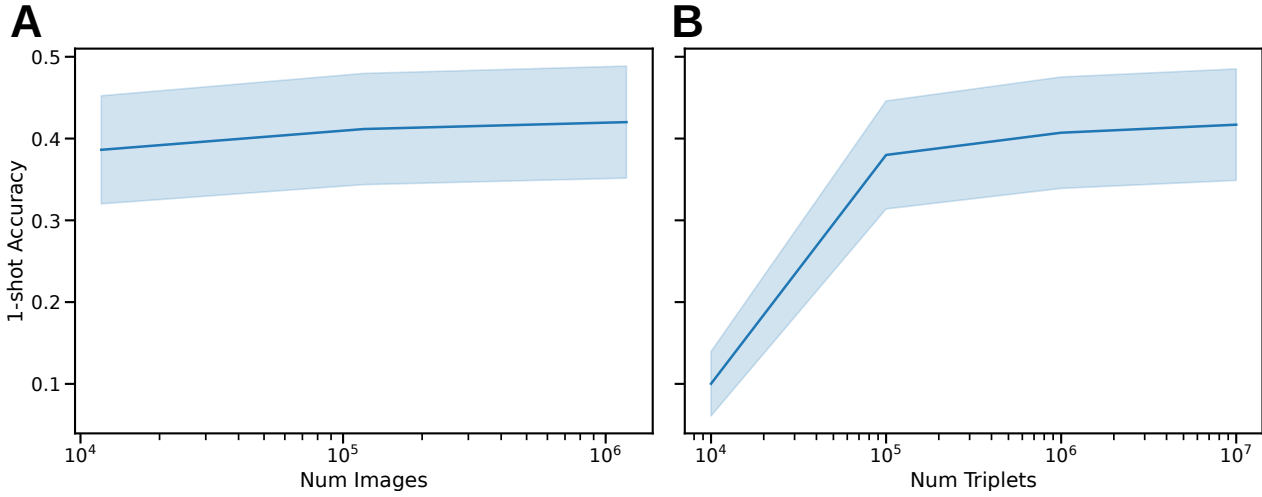


Figure 14 | Accuracy in 1-shot linear probing over a number of common few-shot evaluation datasets when scaling **A** The number of images or **B** the number of triplets. Error bars show the standard error when averaging over datasets.

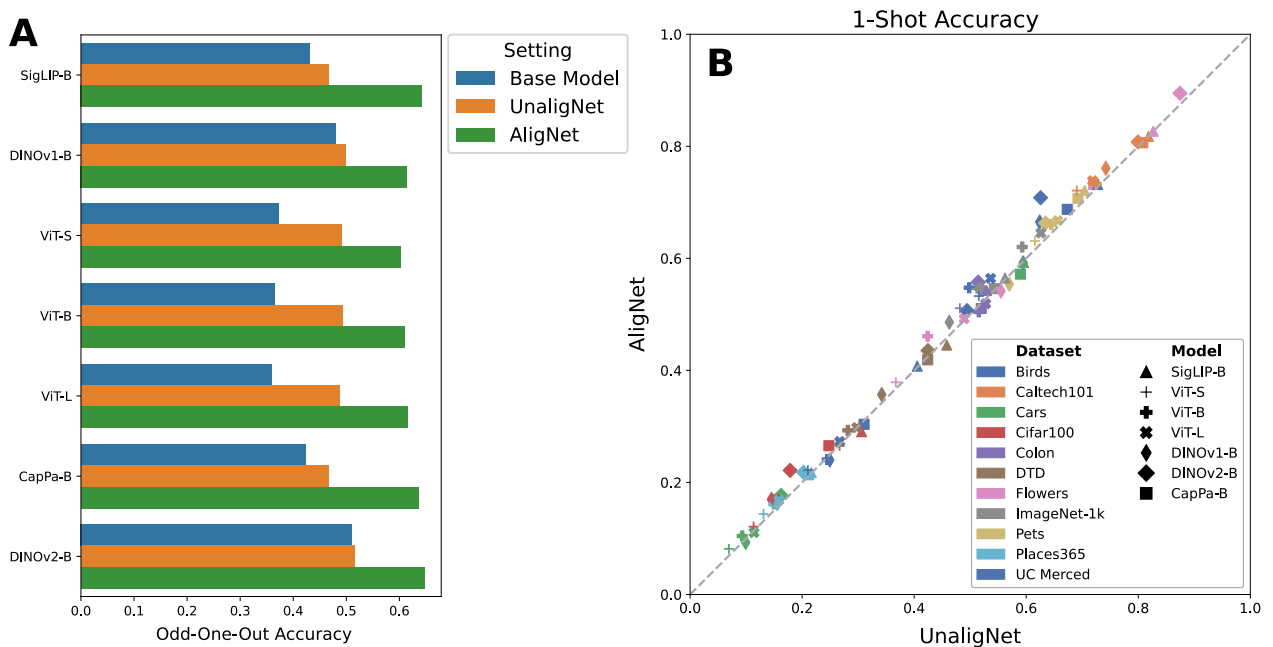


Figure 15 | **A:** Odd-one-out accuracies on the THINGS dataset for different models in different settings. This figure is similar to (an extended version of) the THINGS plot in Fig. 2A. ‘‘AligNet’’ and ‘‘Base Model’’ refer to the pretrained student model, without and with finetuning on AligNet respectively. UnAlignNet refers to a student finetuned on a variant of the AligNet dataset with an unaligned teacher. **B:** Comparing 1-shot accuracy on 11 datasets after fine-tuning on UnalignNet (x-axis) with fine-tuning on AligNet (y-axis). Most points lie slightly above the diagonal indicating that alignment of the teacher leads to a small but significant improvement in 1-shot performance of the student. This ablation shows the importance of aligning the teacher model for getting aligned student models.

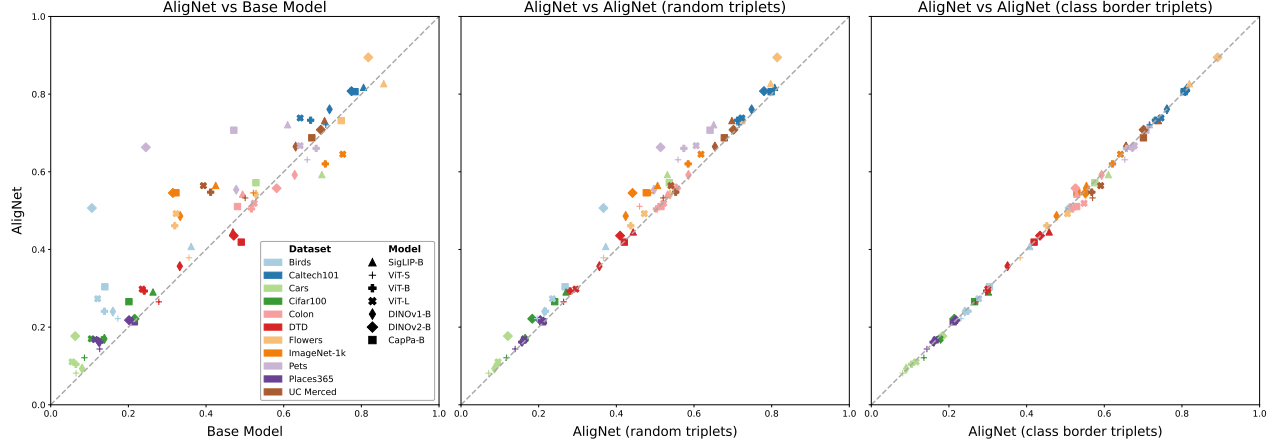


Figure 16 | 1-shot accuracy on various image datasets, comparing performance of an AligNet trained model (y-axis) with three other reference models. **Left:** Again comparing base-model (x-axis) with AligNet (y-axis) for reference. **Middle:** Comparing students fine-tuned using random triplets (x-axis) with AligNet (y-axis). **Right:** Comparing students fine-tuned using class-border triplets (x-axis) with AligNet (y-axis).

large part due to the teacher model and our distillation method. But importantly, the vast majority of remaining improvements are positive, which means that using an aligned teacher gives a consistent advantage over an unaligned teacher.

We confirm the significance of this trend by fitting a repeated measurements ANOVA to the accuracy on the different datasets, and treating the choice of model and the fine-tuning method (AligNet vs UnaligNet) as conditions. Based on this ANOVA, the null-hypothesis that the fine-tuning do not affect the 1-shot accuracy, can be rejected at the  $p < 0.01$  level.

**Investigating different Triplet Sampling Schemes** Sampling triplets is an important part of the AligNet pipeline, and the choice of triplets can greatly influence the effect and efficacy of the student finetuning. Here we compare three different sampling strategies:

- **Cluster-border sampling:** This is the strategy used for AligNet. It is unsupervised and uses a k-means clustering of the teacher representations to sample triplets with two nearby images (same cluster) and one far away image (different cluster).
- **Class-border sampling:** This strategy is analogous to cluster-border sampling, but instead of clusters it uses the ImageNet labels to sample two nearby images (same class) and one far away image (different class).
- **Random sampling:** As a control we also compare to fully random sampling of triplets, i.e. each image is chosen with equal probability from the full set of all images.

Fig. 16 shows the 1-shot accuracy of student models when comparing different sampling strategies. In all three panels, the y-axis corresponds to the performance of a model after AligNet-fine-tuning. The left panel, again shows how this compares to the performance of the (not fine-tuned) base model (x-axis). The middle panel compares shows how AligNet performance compares to fine-tuning on random-triplets (x-axis). Finally, the right panel shows comparison between AligNet and fine-tuning on triplets sampled from class-borders. Notice that the difference in the middle panel between random triplet sampling is consistently and substantially worse than cluster-based sampling. This clearly highlights the importance of the triplet sampling for down-stream performance. The panel on the right, on the other hand, shows that there is virtually no difference between cluster-border sampling and class-border sampling. So when label information is available, that can effectively be used for sampling triplets, but even if there is not, the clustering based sampling will work just as well.

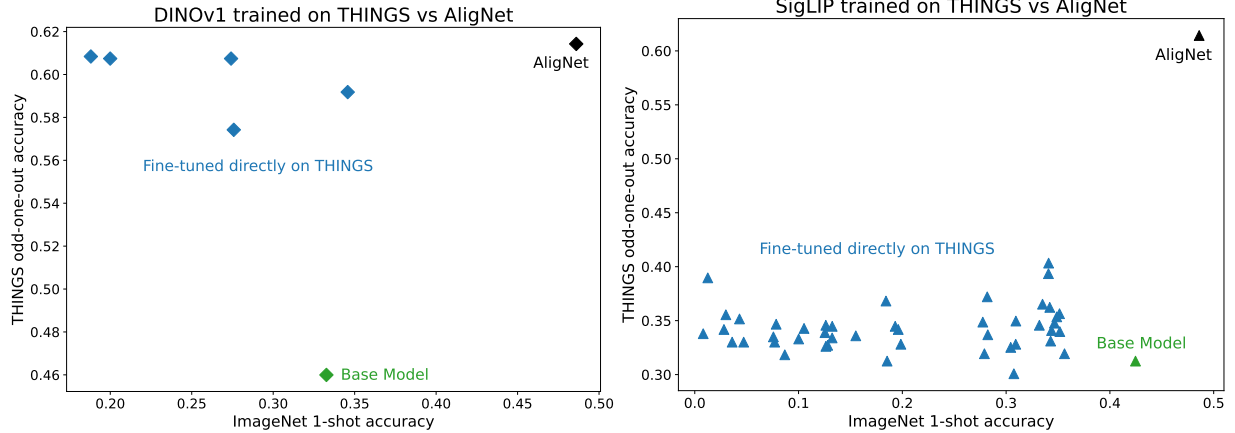


Figure 17 | Performance on two different tasks: ImageNet 1-shot accuracy (x-axis) and odd-one-out accuracy on THINGS (y-axis) for two models (DINOv1 on the left, SigLIP-B on the right). The green markers correspond to the base model, and the black marker to the model fine-tuned on AligNet. The different blue markers in the scatterplot correspond to different hyperparameter settings (learning rate, weight decay, ...) for fine-tuning directly on THINGS.

**Fine-tuning directly on THINGS** We have argued that fine-tuning models to better align them with human similarity judgments depends on having sufficiently large datasets, which do not exist yet. This argument has motivated our multi-stage approach of first linearly aligning teacher model and then using this as a surrogate to generate a large corpus of human-like triplets. Yet, if we look at Fig. 14, it seems that decreasing the number of images or the number of triplets by up to two orders of magnitude still retains most of the benefit on downstream performance (in terms of few-shot accuracy). This raises the question, whether our pipeline as a whole might be unnecessary, given that the THINGS [Hebart et al., 2023] dataset already contains 4.70 million human similarity judgments collected via online crowd- sourcing for 1854 object images. In this section, we therefore compare AligNet based training with just using the THINGS odd-one-out triplets directly for fine-tuning of student models. Fig. 17 shows that fine-tuning directly on THINGS is consistently worse than training on AligNet in terms of ImageNet 1-shot accuracy (x-axis). Importantly, it appears that in almost all cases the performance of the model actually decreased below that of the base model. It is also interesting, that even in terms of THINGS odd-one-out accuracy, the AligNet trained model performs better than the any other model. This is somewhat surprising, because it means that there is an overfitting problem when training on THINGS, that seems to mostly disappear when training on AligNet.

### B.3. Qualitative Analysis of Representations

#### B.3.1. Principal Components Analysis of Representations

In Fig. 18 we show PCA projections of the space of image representations from four different models before and after fine-tuning on AligNet. It shows that the large-scale structure of the representational space becomes more structured and interpretable. Notice for example that animals (blue) and food (green) are clearly separated from artifacts such as furniture (red), musical instruments (purple) and clothing items (orange) which are much more clustered together. The same structuring effect — though to a lesser degree — can be seen for principal components three and four (see Fig. 19).

This increased structuring within the first few principal components is also reflected in the amount of variance explained by them. The third row of Fig. 18 clearly shows a notable increase of the proportion of the total variance of the representations that can be explained with only the first 5-15 principal components. It is also striking how different the global structure of the four models is before

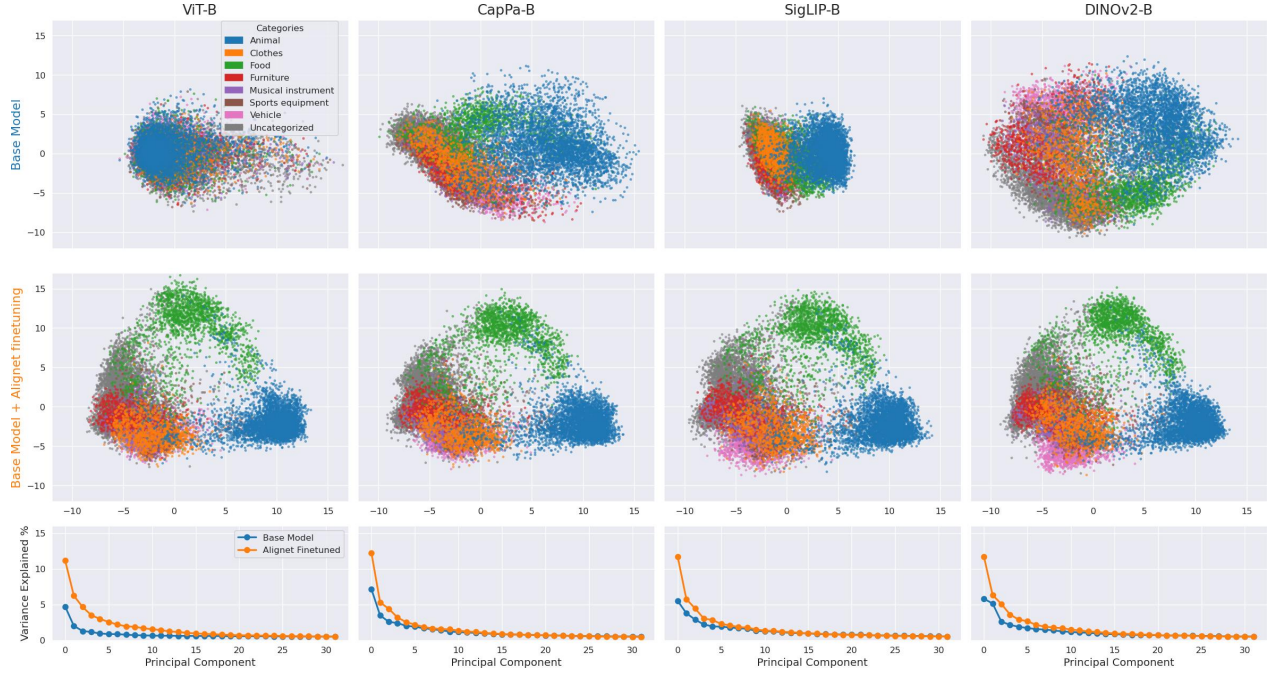


Figure 18 | Projection of the representations of 85k ImageNet images from four different models (columns) onto their first two principal components both before (first row) and after fine-tuning on AlignNet (second row). Colors correspond to high-level categories of the images. The third row visualizes the proportion of explained variance for the first 32 principal components.

fine-tuning on AlignNet, and how similar it becomes afterwards.

In Fig. 20 we further show projections of the representations using TriMap [Amid and Warmuth, 2019], which is a non-linear dimensionality reduction technique designed to better preserve both the global and the local structure of the data. While the coarse structure is similar to that of the first two PC (see Fig. 18), the fine-grained structure reveals some interesting details. Note for example that in the TriMap projection the ViT-B exhibits a lot of fine-grained structure in the form of tiny clusters.

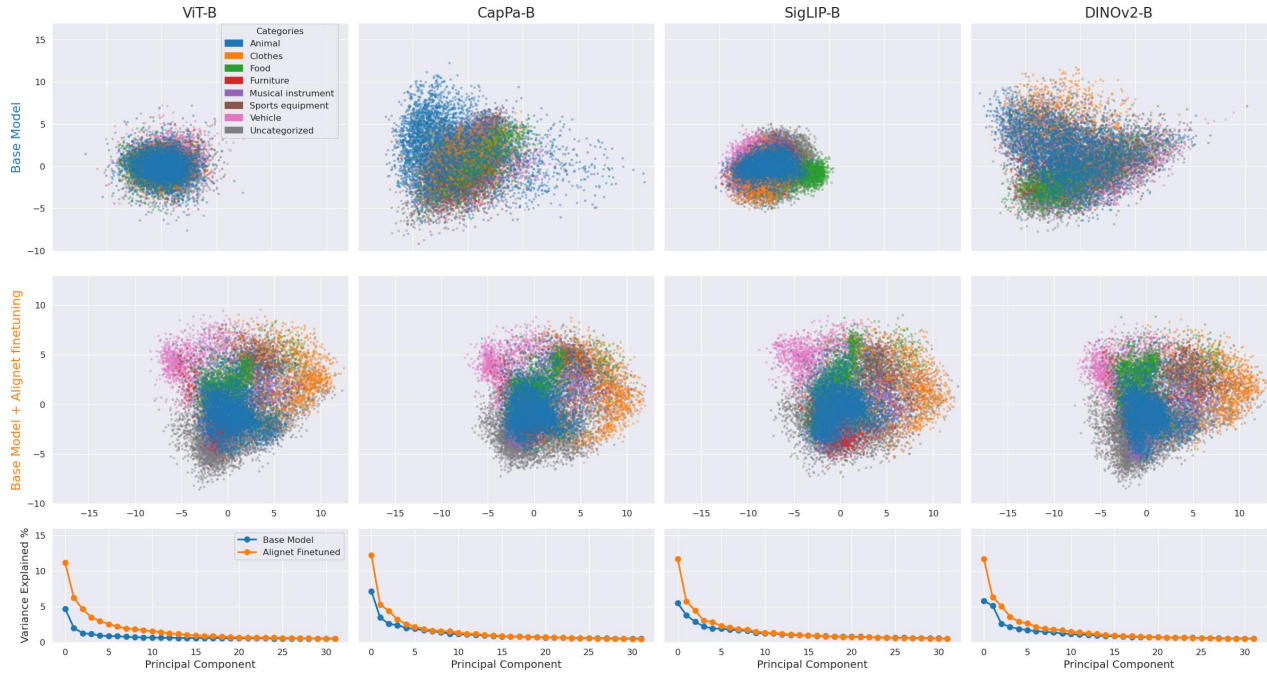


Figure 19 | Projection of the representations of 85k ImageNet images from four different models (columns) onto their first two principal components both before (first row) and after fine-tuning on AlignNet (second row). Similar to Fig. 18 but for components 3 & 4.

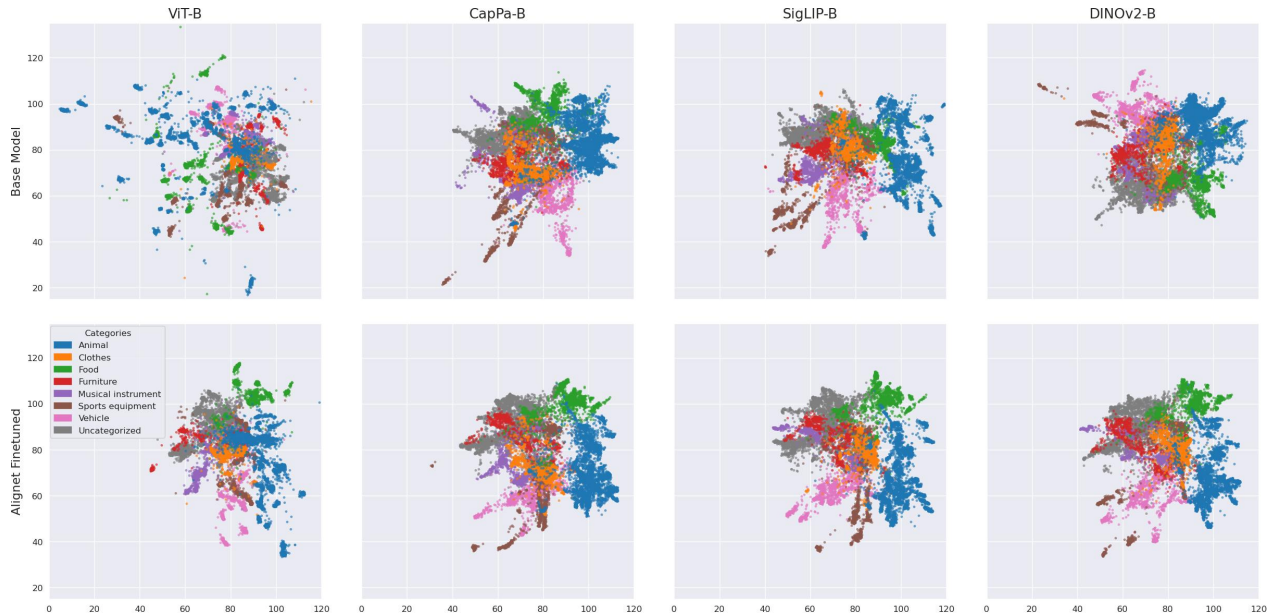


Figure 20 | Projection of the representations of 85k ImageNet images from four different models (columns) onto 2 dimensions using TriMap [Amid and Warmuth, 2019] both before (first row) and after fine-tuning on AlignNet (second row). Colors correspond to high-level categories of the images.

### B.3.2. Detailed results on alignment with the semantic hierarchy

In Fig. 21 we show the distribution of changes in relative distance between the representations of pairs of ImageNet images for four models. We measure this distance change relative to other changes (by  $z$ -scoring), because relative distances are more meaningful than absolute ones (e.g., scaling all representations by a factor of two would change absolute distances, but not relative ones), and absolute scales of all representations tend to increase during training.

In general, images from classes that come from the same superordinate category (such as two different species of bird) tend to end up relatively closer together, while those from different superordinate categories tend to end up farther apart. The exact distribution of changes depends on the prior representation structure of the models; the effect is stronger for models that had lower-quality initial representations.

In Fig. 22 we show a more detailed visualization, showing a matrix of average changes in the relative distances between a subset of the *basic-level* categories, grouped into several higher-level semantic categories (animals, clothes, food, furniture, musical instruments, sports equipment, and vehicles), which are plotted as blocks on the diagonals. The block structure of the changes is clear, with overall increases in similarity within these broad categories, and decreases in similarity between them.

Taken together, these results show qualitatively that our alignment process is working as intended—it is reorganizing the representation space of the model in accordance with the structure of human semantic knowledge.

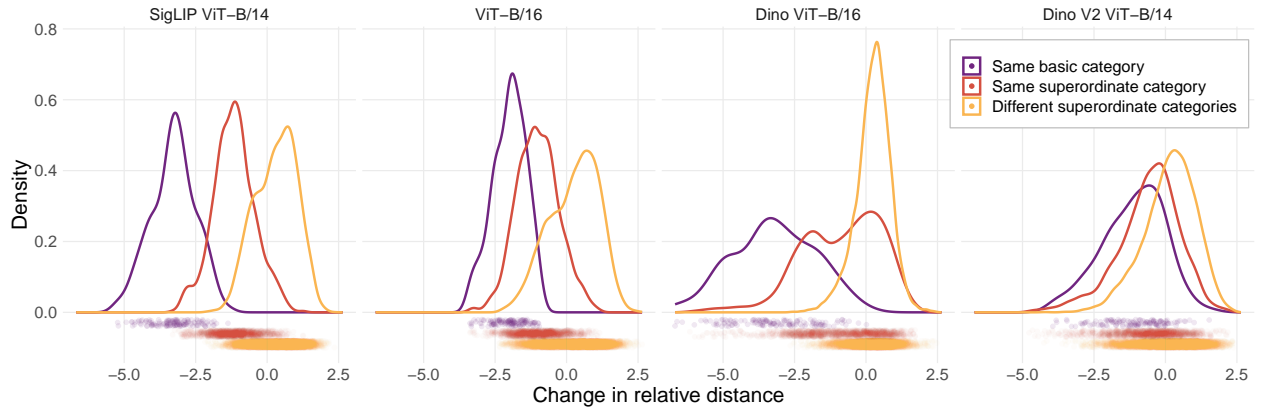


Figure 21 | Changes in relative distances between stimuli reflect the superordinate category structure. Representations within the same superordinate category tend to end up relatively closer together than those in different superordinate categories.

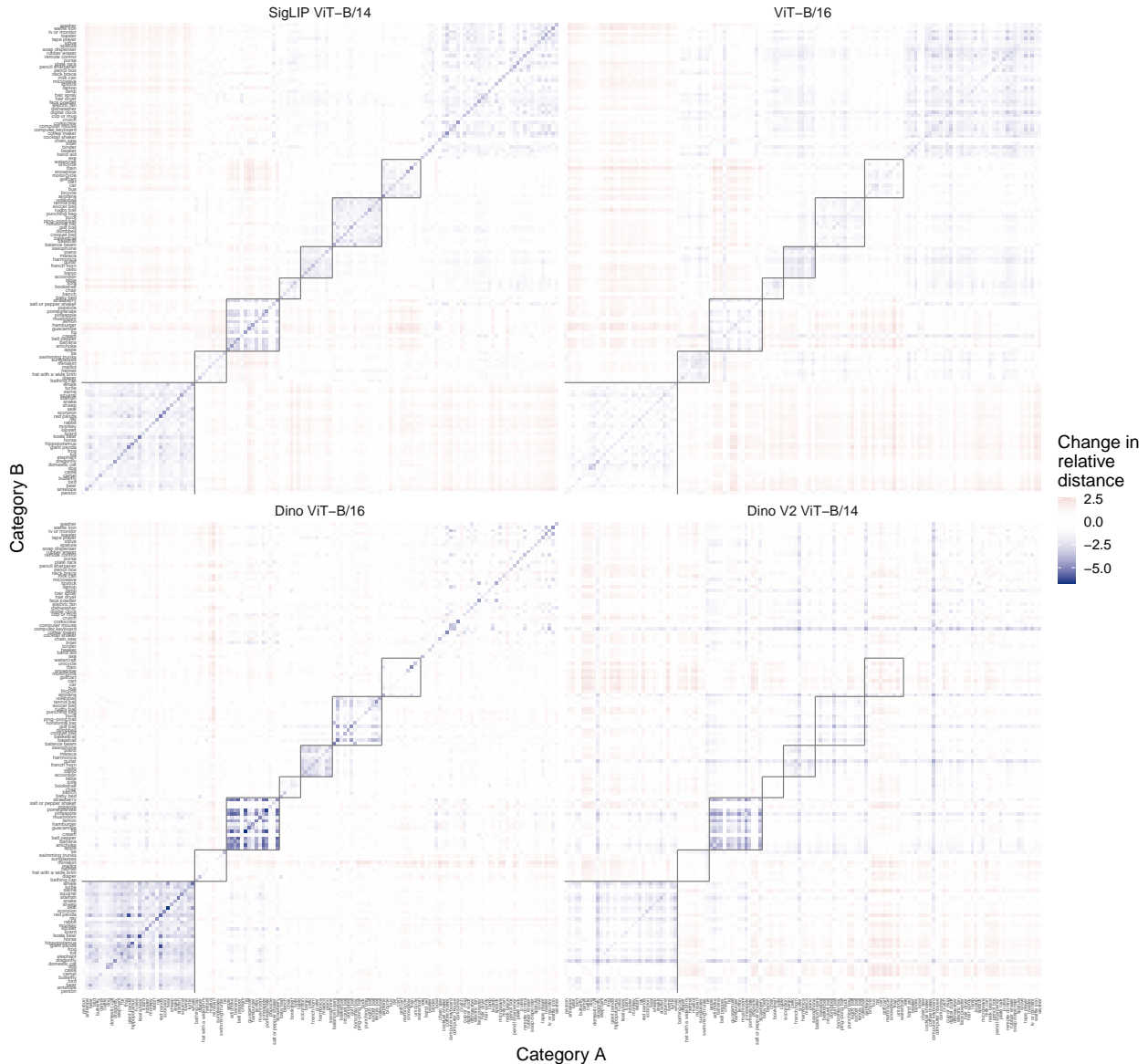


Figure 22 | Changes in relative distances between stimuli are structured by higher-level semantics. After alignment, representations end up relatively more similar to one another within broad categories (diagonal blocks)—particularly human-salient ones like “animals” or “food”—and less similar between these categories.